

HyperNetWalk: A Unified Framework for Personalized and Population-Level Cancer Driver Gene Identification via Multi-Network Hypergraph Diffusion

Xueqing Xu^{1,2}, Yonghang Gao^{1,2}, Duanchen Sun^{3,*}, and Ling-Yun Wu^{1,2,*}

¹*State Key Laboratory of Mathematical Sciences, Academy of Mathematics and Systems Science, Chinese Academy of Sciences, Beijing 100190, China*

²*School of Mathematical Sciences, University of Chinese Academy of Sciences, Beijing 100049, China*

³*School of Mathematics, Shandong University, Jinan 250100, China*

**Correspondence: dcsun@sdu.edu.cn (D. Sun); lywu@amss.ac.cn (L.-Y. Wu)*

Abstract

Identifying cancer driver genes is crucial for understanding tumor biology and developing precision therapies. However, existing computational methods often rely on single biological networks or population-level mutation patterns, limiting their ability to identify patient-specific drivers and leverage the complementary information from multiple network types. Here, we present HyperNetWalk, a novel computational framework that integrates multiple biological networks and hypergraph diffusion to identify driver genes at both personalized and cohort levels. In the first stage, HyperNetWalk integrates protein-protein interaction networks, gene regulatory networks, and dynamic co-expression networks through sample-independent random walks on patient-specific subnetworks to capture topological importance and expression perturbation effects. In the second stage, it refines predictions through hypergraph-based random walks that leverage cross-sample information while preserving individual mutational contexts. Comprehensive evaluation on 12 TCGA cancer types demonstrates that HyperNetWalk achieves superior or competitive performance compared to state-of-the-art methods in both personalized and cohort-level predictions. Notably, HyperNetWalk successfully identifies known driver genes with high precision while revealing cancer type-specific drivers that reflect distinct biological mechanisms. Our framework provides a unified solution for personalized and population-based driver gene identification, offering valuable insights for precision oncology and therapeutic target discovery.

1. Introduction

Cancer is one of the most deadly diseases in the world, which is initiated by the accumulation of somatic mutations in the genome. The mutations that can confer a selective growth advantage to tumour cells are called driver mutations, while the others are referred to as passenger mutations. And genes that harbour driver mutations are called cancer driver genes. Due to the high heterogeneity and the existence of a huge number of passenger genes, identifying cancer driver genes has been a classical challenge in cancer research, which is valuable for reducing cancer morbidity and mortality. With the development of biotechnologies, larger amounts and more diverse types of cancer-related data have become more readily available for research. For instance, the Cancer Genome Atlas (TCGA) and Cancer Cell Line Encyclopedia (CCLE) are commonly used databases that contain multi-omics data across various cancer types.

Based on these available resources, many approaches for cancer driver gene identification have emerged in these years.

The first kind of methods are the mutation frequency-based methods, with the hypothesis that the driver genes tend to mutate more frequently than passenger genes. Thus, these methods always need to estimate the background mutation rate (BMR) accurately. This kind of methods include MutSigCV [1], which corrects for patient-specific and gene-specific heterogeneity by incorporating gene expression level and DNA replication time; DriverML [2], which uses a machine learning model to predict driver genes based on multiple features, including mutation frequency, functional impact of mutations, and mutation clustering. However, since only a small fraction of driver genes are frequently mutated, these methods may neglect the rarely-mutated driver genes.

Some methods are based on the functional impact of mutations, which assume that driver mutations tend to have higher functional impact than passenger mutations, such as OncodriveFML [3] and MutPan-ning [4]. Although these methods can identify some rarely-mutated driver genes, they are computationally intensive and may need high-quality functional annotations.

Since cancer is a complex disease that involves multiple genes and pathways, some network-based methods have been proposed to identify driver genes by integrating various biological networks, such as the protein-protein interaction (PPI) network and gene regulatory network (GRN). And with the development of graph neural networks (GNNs), there are many GNN-based methods for driver gene identification, like EMOGI [5] and IMI-driver [6]. However, since methods based on GNNs almost treat the identification of driver genes as a node classification problem with a homophily assumption, which cannot fully capture the unique characteristics of driver genes, they need sufficient labelled data for training and thus are always used for pan-cancer cases. While unsupervised methods can overcome the unbalanced and incomplete labelled data problem, they can be better candidates for the problem. For example, HotNet2 [7] identifies significantly mutated subnetworks on the PPI network by using a heat diffusion process; DriverNet [8] constructs a bipartite graph between mutated genes and differentially expressed genes (DEGs) based on the PPI network and identifies driver genes by solving an integer linear programming problem. These methods can effectively utilize the topological properties of biological networks to identify driver genes.

As one of the main characteristics of cancer is the high heterogeneity, different patients with the same cancer type may have different driver genes [9]. Therefore, many personalized methods have been proposed to identify driver genes for individual patients. DawnRank [10] constructs a personalized gene interaction network for each patient based on the PPI network and DEGs, and then uses a modified PageRank algorithm to rank the mutated genes; SCS [11] identifies a minimal set of mutated genes that can cover all DEGs in a personalized gene interaction network by solving a combinatorial optimization problem. These methods can effectively capture the individual-specific characteristics of cancer and thus identify personalized driver genes. However, they may not fully utilize the information from other patients with similar cancer types. PersonaDrive [12] constructs a personalized bipartite graph between mutated genes and DEGs for each patient, and then uses a random walk with restart algorithm to score the mutated genes based on their connectivity to DEGs with incorporating cohort information into the personalized graph. PDRWH [13] first builds a patient-specific hypergraph by integrating mutated genes and DEGs of the patient and other patients with similar mutation profiles, and then uses a random walk algorithm on the hypergraph to rank the mutated genes.

However, most existing network-based approaches rely on a single type of biological network—typically the PPI network—making their performance vulnerable to network incompleteness and noise. Integrating multiple types of biological networks may not only alleviate this problem but also provide complemen-

tary information for identifying driver genes. In fact, DriverMP [14] has integrated the PPI network and differential expression network to identify driver genes by estimating mutated gene pairs first. IMI-driver [6] has utilized GNN to integrate multi-omics data and multiple biological networks, including the PPI network, TF-target network, co-expression network, and ceRNA network, to predict driver genes. However, these methods can only identify the cohort-level driver genes, which may lack precision and fine-granularity. To address these limitations, we propose HyperNetWalk, a novel unsupervised framework that integrates both static biological networks (PPI and GRN) and dynamic co-expression networks to identify cancer driver genes at both the personal and cohort levels. HyperNetWalk employs a two-stage random walk strategy: the first stage prioritizes mutated genes within multiple complementary networks, and the second stage incorporates cross-sample information through a hypergraph-based random walk to refine predictions. We applied HyperNetWalk to 12 TCGA cancer types and a pan-cancer dataset. The results show that HyperNetWalk achieves performance comparable to state-of-the-art methods, while uniquely providing both personalized and cohort-level predictions within a unified framework.

2. Results

2.1 Overview of HyperNetWalk framework

HyperNetWalk is an unsupervised two-stage framework that integrates multi-omic signals and multi-type biological networks to prioritize candidate driver genes at both the individual and cohort levels (see Fig.1). The model combines network diffusion on sample-specific subnetworks with hypergraph-based aggregation across patients to provide multi-evidence driver predictions.

Stage I: Sample-independent Random Walks. For each patient, two types of subnetworks are constructed: (i) *static networks* derived from public databases, including PPI and GRN, and (ii) a *dynamic co-expression network* inferred from tumor and normal expression profiles. Patient-specific subnetworks are induced using the patient’s mutated genes and, for the dynamic network, differentially expressed genes (DEGs). Random walks with restart (RWR) are independently performed on each network to capture complementary aspects of driver activity—topological prominence in static networks and expression-perturbation relevance in the dynamic network. The resulting steady-state distributions are integrated into an initial per-gene driver score for each patient.

Stage II: Hypergraph Random Walks. In the second stage, cross-patient information is incorporated through hypergraph diffusion. For individual-level prediction, a patient-specific hypergraph is built in which nodes represent mutated genes and hyperedges correspond to the patient together with its most similar neighbors. Node weights are set according to the Stage I scores, and a hypergraph random walk with restart is applied to refine patient-specific driver rankings. For cohort-level prediction, a single hypergraph containing all patients is constructed, enabling population-level diffusion and cohort-level prioritization.

Collectively, HyperNetWalk integrates (i) topology-aware diffusion on static networks, (ii) perturbation-oriented diffusion on dynamic co-expression networks, and (iii) hypergraph diffusion across patients. This multi-evidence integration provides interpretable and robust driver gene rankings at both individual and cohort scales.

2.2 HyperNetWalk leverages the characteristic topological properties of driver genes

To validate the biological rationale underlying HyperNetWalk’s network-based approach, we examined whether known driver genes exhibit distinct topological properties compared to other mutated genes.

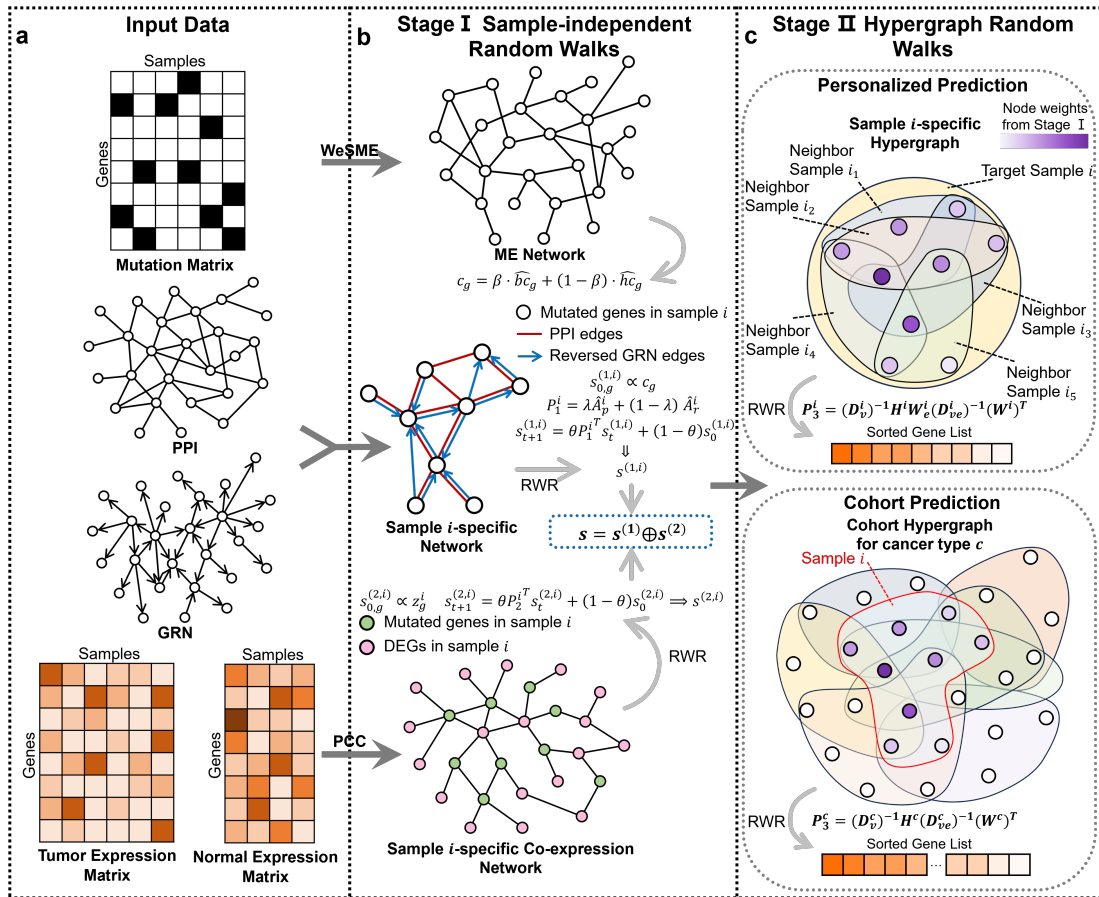


Figure 1. Overview of HyperNetWalk. (a) HyperNetWalk integrates a somatic mutation matrix, gene expression matrix from tumor and normal samples, a protein–protein interaction (PPI) network, and a gene regulatory network (GRN) as inputs. (b) In Stage I, sample-independent random walks with restart are performed on patient-specific subnetworks derived from the PPI, GRN, and dynamic co-expression networks to generate initial per-gene driver scores for each patient. (c) In Stage II, hypergraph random walks with restart are applied to refine driver rankings at both the individual and cohort levels by incorporating cross-patient information.

For each cancer type, we classified mutated genes into known drivers (present in CGC Tier 1) and non-drivers, and compared their network characteristics.

The first stage of HyperNetWalk integrates topological information from PPI and GRN. We therefore evaluated the degree distribution in the PPI network and the out-degree distribution (regulatory capacity) in the GRN for both groups. As shown in Figure S1 (a, b), known driver genes consistently exhibit significantly higher degrees and out-degrees than non-drivers across all 12 cancer types and the pan-cancer cohort. This elevated centrality indicates that driver genes tend to occupy hub positions in both interaction and regulatory networks, supporting the biological basis for incorporating these networks into driver gene identification.

HyperNetWalk can optionally incorporate centrality information from cancer type-specific mutual exclusivity (ME) networks as prior information when the ME network is sufficiently large ($|V_m^c| \geq 200$). To assess whether ME networks capture meaningful biological signals, we compared the betweenness centrality and harmonic centrality of known drivers versus non-drivers in these networks. Among the 12 cancer types evaluated, five have sufficiently large ME networks for analysis. As shown in Figure S1 (c, d), known drivers demonstrate significantly higher betweenness centrality in all five cancer types, reflecting their importance as connectors in the ME network. For harmonic centrality, four out of five cancer types

show significantly higher values for known drivers, with only LUAD deviating from this pattern. These results suggest that ME-derived centrality provides biologically meaningful prior information for most cancer types with sufficient mutational data.

Finally, we examined whether HyperNetWalk successfully leverages these topological properties to prioritize known driver genes. We compared the predicted ranks of known drivers versus non-drivers at both the personalized (patient-specific) and cohort levels. As shown in Figure S1 (e, f), known driver genes receive significantly better (lower) ranks than non-drivers in both evaluation settings across all cancer types. The consistent and substantial ranking differences demonstrate that HyperNetWalk effectively integrates network topology and expression perturbation information to identify biologically meaningful driver candidates.

2.3 HyperNetWalk delivers high-confidence predictions at both personalized and cohort levels

We benchmarked HyperNetWalk against widely used personalized methods (DawnRank [10], PersonalDrive [12], PDRWH [13], PITCH [15], PRODIGY [16]) and cohort-level methods (DriverMP [14], DriverRWH [17], Subdyquency [18]). Given that effective driver gene identification requires prioritizing a small number of high-confidence candidates from a large pool of mutations, our evaluation focuses on top-ranked predictions. For cohort-level analysis, we calculated metrics based on the top 200 ranked genes. For individual-level analysis, we followed the ranking-evaluation-aggregation (REA) strategy [12], evaluating the top N_c predictions per cancer type, where N_c equals twice the median number of true driver genes per sample in that cohort. Detailed evaluation protocols and metrics are described in Methods.

On the individual level, HyperNetWalk demonstrates robust performance across the 12 TCGA cancer types. As illustrated in the Precision@K curves (Fig. 2), HyperNetWalk consistently ranks among the top performers. While DawnRank exhibits strong performance and achieves the highest precision in certain cancer types, HyperNetWalk consistently delivers competitive results that are comparable to DawnRank across the majority of datasets. This competitiveness is further supported by the Recall@K and F1-score@K evaluations (see Supplementary Fig. S2 and Fig. S3, respectively). These results indicate that HyperNetWalk is a highly reliable alternative for personalized analysis, capable of capturing critical driver signals with high stability.

On the cohort level, the performance landscape is led by DriverMP, which is explicitly designed to capture population-wide mutation patterns. However, HyperNetWalk consistently outperforms all other baseline methods, establishing itself as the second-best performer. This trend is evident across multiple metrics, including Precision@K (Fig. 3), Recall@K (Supplementary Fig. S4), and F1-score@K (Supplementary Fig. S5). Crucially, comparisons with purely personalized methods (aggregated for cohort evaluation) reveal that HyperNetWalk significantly surpasses them in identifying population-level drivers.

To further evaluate the model's ability to prioritize top-ranked candidates—a critical requirement for driver gene identification which effectively constitutes an imbalanced classification problem—we summarized the AUPRC, AUROC, partial AUPRC (pAUPRC), and partial AUROC (pAUROC) in Table S2. Additionally, the corresponding Precision-Recall and ROC curves are provided in Supplementary Fig. S6 and Fig. S7. Given the class imbalance, pAUPRC and pAUROC are particularly suitable for assessing precision among top-ranked predictions. In terms of pAUPRC, HyperNetWalk and DriverMP consistently emerge as the top two methods nearly across all 12 cancer types, with HyperNetWalk ranking marginally lower than DriverMP but significantly higher than other baselines. Regarding pAUROC, HyperNetWalk achieves performance comparable to the personalized method DawnRank. However, as evidenced by the Precision@K plots, DawnRank's precision tends to drop more rapidly in the top-ranked list compared to

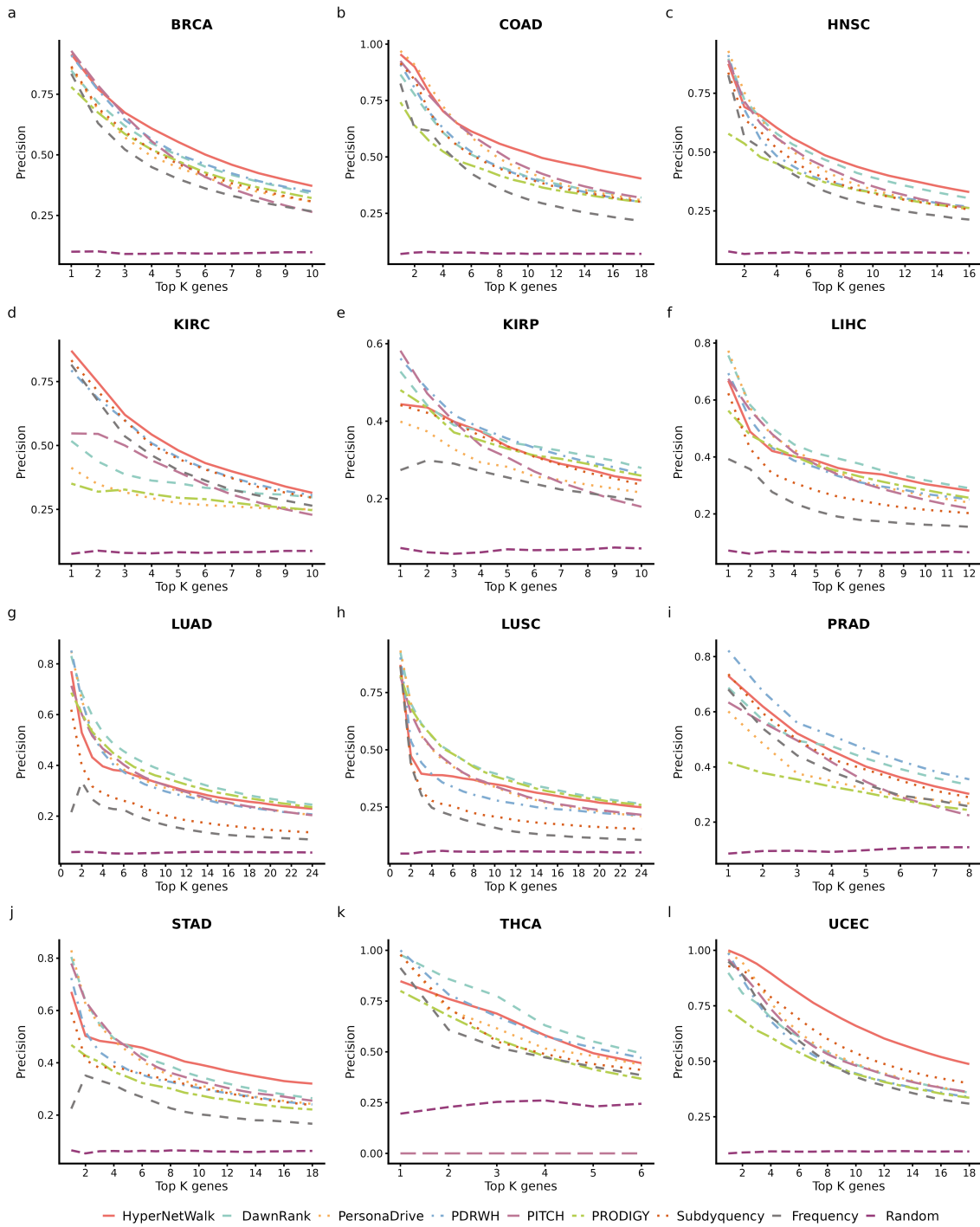


Figure 2. Personalized prediction performance: Precision@K across cancer types. Precision@K curves for HyperNetWalk and baseline methods on personalized driver gene identification across 12 TCGA cancer types. Panels (a–l) represent different cancer types, showing how precision varies with the number of top-ranked predictions (K). Performance is evaluated on the top N_c predictions for each cancer type, where N_c is cancer type-specific and adaptively set based on the expected number of drivers per sample (see Methods). HyperNetWalk (pink line) consistently achieves competitive or superior precision across most cancer types, demonstrating robust performance in identifying patient-specific driver genes.

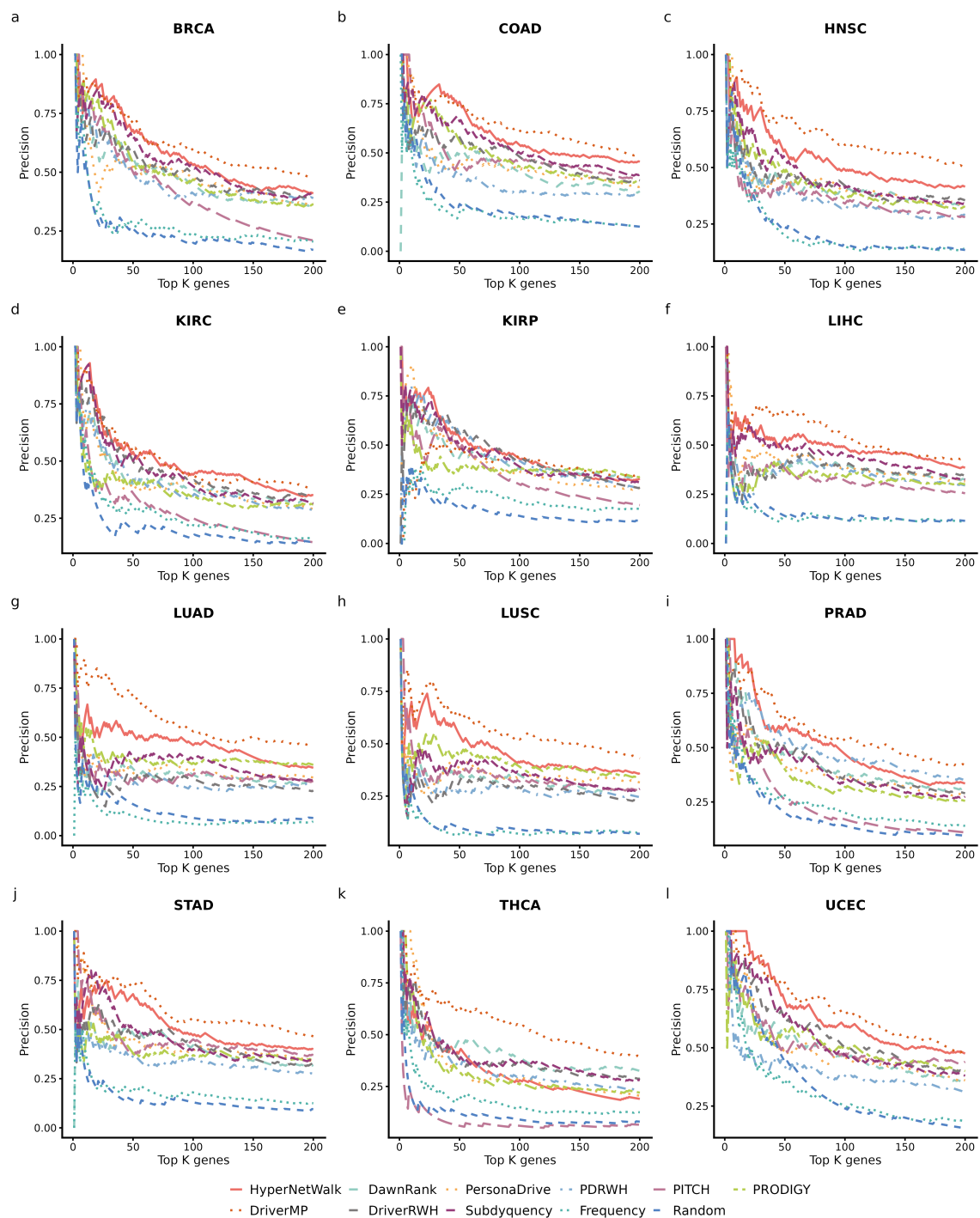


Figure 3. Cohort-level prediction performance: Precision@K across cancer types. Precision@K curves for HyperNetWalk and baseline methods on cohort-level driver gene identification across 12 TCGA cancer types. Panels (a–l) represent different cancer types. Performance is evaluated on the top 200 predicted driver genes to prioritize high-confidence candidates suitable for experimental validation. HyperNetWalk consistently ranks as the second-best method after DriverMP, substantially outperforming all other baseline methods, including aggregated personalized methods.

HyperNetWalk in several datasets. This suggests that HyperNetWalk is particularly effective at prioritizing high-confidence candidates at the very top of the list, which is practically valuable for downstream experimental validation.

The distinct advantage of HyperNetWalk lies in its versatility. Existing approaches often face a trade-off: cohort methods like DriverMP lack patient-specific resolution, while personalized methods like DawnRank may not explicitly optimize for population-level consensus. HyperNetWalk effectively bridges this gap. By integrating multitype networks with hypergraph diffusion, it achieves performance comparable to state-of-the-art methods in their respective domains—remaining competitive with DawnRank individually and DriverMP globally—while offering the unique capability to provide high-confidence predictions at both levels simultaneously within a unified framework.

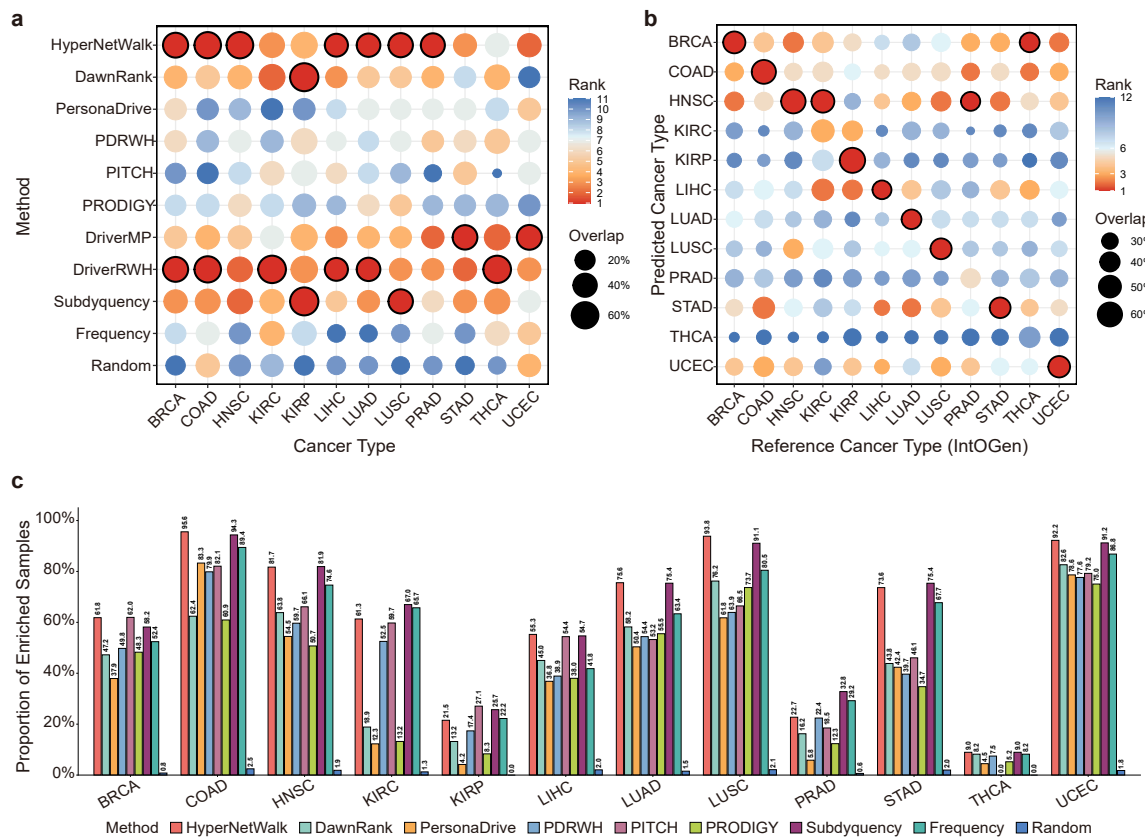


Figure 4. Evaluation of cancer-type specificity using IntOGen driver genes. (a) Comparison of cohort-level performance across different methods. The top 200 predictions from each method were tested for enrichment in cancer-specific drivers. Dot size indicates the overlap ratio (recall), while color represents the enrichment significance rank within each cancer type (red indicates Rank 1/Best Match). The most significant predictions for each cancer type are highlighted with black circles. (b) Cross-cancer specificity assessment for HyperNetWalk. The y-axis represents the predicted cancer type, and the x-axis represents the IntOGen reference set. A distinct diagonal pattern indicates high tissue specificity. (c) Performance of individual-level predictions. The bar chart shows the proportion of valid samples (harboring known specific drivers) where the top- N_c predictions significantly enriched for cancer-specific drivers ($P < 0.05$).

2.4 HyperNetWalk captures cancer-type-specific driver landscapes at both cohort and individual levels

While the CGC Tier 1 list provides a benchmark for general driver genes, cancer is a highly heterogeneous disease driven by tissue-specific mechanisms. Therefore, evaluating the ability to identify

cancer-specific drivers is crucial. To this end, we utilized the IntOGen database, which offers a curated compendium of driver genes specific to distinct cancer cohorts.

For cohort-level evaluation, we assessed the enrichment of the Top-200 predictions from various methods in cancer-specific driver sets using hypergeometric tests. As shown in Fig. 4(a), HyperNetWalk consistently achieves superior performance across almost all cancer types, visualized by the largest node sizes (highest overlap proportion) and red coloring (top-ranked significance). Notably, HyperNetWalk outperforms the aggregated predictions from personalized methods and remains highly competitive against cohort-based methods. It even surpasses DriverMP—a strong baseline in general benchmarking—in identifying specific drivers for several cancer types (e.g., BRCA and COAD).

To rigorously verify that HyperNetWalk captures tissue-specific signals rather than merely prioritizing pan-cancer drivers (e.g., *TP53*), we conducted a cross-cancer specificity analysis (Fig. 4(b)). In this specificity matrix, we compared the enrichment of HyperNetWalk’s predictions on a specific cancer type against reference sets from all cancer types. The results exhibit a striking diagonal pattern, where the diagonal elements (matched cancer types) almost consistently show the highest relative enrichment ranking and substantial overlap. This confirms that HyperNetWalk successfully learns cancer-specific topological features and does not rely solely on identifying general driver genes.

Complementing the cohort-level analysis, we further evaluated the performance of HyperNetWalk at the individual sample level. We filtered for valid samples containing at least one known specific driver and sufficient mutation burden to ensure statistical validity. Fig. 4(c) summarizes the proportion of samples successfully enriched for cancer-specific drivers within the top- N_c predictions. HyperNetWalk achieves the highest enrichment proportion across the majority of cancer cohorts, demonstrating its robustness in identifying driver events in individual patients, even when restricted to a strictly defined cancer-specific search space.

3. Methods

3.1 Datasets

Somatic mutation and gene expression profiles were obtained from The Cancer Genome Atlas (TCGA) project. TCGA provides multi-omic data across 33 cancer types. In this study, we analyzed 12 tumor types for which gene expression data included at least 30 normal samples: BRCA, COAD, HNSC, KIRC, KIRP, LIHC, LUAD, LUSC, PRAD, STAD, THCA, and UCEC. The data were downloaded from the UCSC Xena platform [19], which hosts uniformly processed TCGA datasets to ensure comparability across cancer types. Detailed statistics of the 12 cancer types are provided in Supplementary Table S1.

Somatic mutation profiles were processed into binary gene-by-sample matrices, indicating whether a gene harbors one or more non-silent mutations in a given patient. Gene expression profiles were directly obtained from Xena, already TPM-normalized and log-transformed.

The protein–protein interaction (PPI) network was obtained from STRING (version 12.0) [20]. STRING integrates experimentally validated and computationally predicted protein associations. We retained interactions with a confidence score greater than 0.4, resulting in a PPI network containing 19,488 proteins and 929,472 interactions.

The gene regulatory network (GRN) was downloaded from RegNetwork [21], which compiles transcriptional and post-transcriptional regulatory relationships curated from multiple sources. We extracted directed regulatory interactions between human transcription factors and target genes, yielding a GRN with 32,919 genes and 1,111,313 directed edges.

3.2 Input Representation

Based on the datasets described above, we formalize the inputs used in our model. For each cancer type, the somatic mutation and gene expression data, along with the PPI and GRN networks, are represented mathematically as follows.

For a given cancer type c , let the somatic mutation matrix be denoted as $M^c \in \{0, 1\}^{m \times n_c}$, where m is the number of genes and n_c is the number of tumor samples for cancer type c . Each entry $M_{ij}^c = 1$ indicates that gene i harbors one or more non-silent mutations in sample j , and $M_{ij}^c = 0$ otherwise. Only patients with at least three mutated genes are retained for further analysis. The tumor and normal gene expression matrices are represented as $X_T^c \in \mathbb{R}^{l \times n_c}$ and $X_N^c \in \mathbb{R}^{l \times n_0^c}$, respectively, where l is the number of genes and n_0^c is the number of normal samples for cancer type c . The tumor samples included in this study must have both somatic mutation and gene expression data available.

The protein–protein interaction network is represented as an undirected graph $G_p = (V_p, E_p)$, where V_p is the set of proteins and E_p is the set of protein–protein interactions. The gene regulatory network is represented as a directed graph $G_r = (V_r, E_r)$, where V_r is the set of genes and E_r is the set of directed regulatory interactions from transcription factors to target genes.

3.3 Sample-independent Random Walks

In this stage, HyperNetWalk conducts random walks with restart on sample-specific subnetworks constructed from the PPI network, GRN, and dynamic co-expression network for each patient individually. This stage aims to prioritize mutated genes based on their topological importance and expression perturbation relevance within each patient’s context. Importantly, this stage can be conducted for each patient independently and in parallel, without utilizing mutation information from other patients.

For a patient sample i of cancer type c , we construct sample-specific subnetworks from two categories of biological networks: (1) *static networks*, including the PPI network G_p and GRN G_r , and (2) *dynamic co-expression network*, inferred from tumor and normal expression profiles.

3.3.1 Random Walks on Static Networks with ME Prior

Let MG_i^c denote the set of mutated genes in sample i . We first induce subnetworks from the PPI network and GRN using the mutated genes. The induced subnetwork from the PPI network is defined as $G_p^i = G_p[MG_i^c]$, which includes all mutated genes and the interactions present in G_p . Similarly, the induced subnetwork from the GRN is defined as $G_r^i = G_r[MG_i^c]$. When constructing G_r^i , we reverse the edge directions in G_r to account for the regulatory potential of driver genes.

We then perform random walks that integrate both networks. At each step, if the current node is u , the random walker transfers to a neighbor in G_p^i with probability λ or to a neighbor in G_r^i with probability $1 - \lambda$. After selecting a network, the walker uniformly chooses one of the neighbors in that network. For isolated nodes (with degree zero in both networks), the walker immediately restarts according to the restart distribution. The transition probability from node u to node v is:

$$P_{1,uv}^i = \lambda \frac{a_{p,uv}^i}{\sum_{k \in MG_i^c} a_{p,uk}^i} + (1 - \lambda) \frac{a_{r,uv}^i}{\sum_{k \in MG_i^c} a_{r,uk}^i}, \quad (1)$$

where $a_{p,lk}^i = 1$ if nodes l and k are adjacent in G_p^i and $a_{p,lk}^i = 0$ otherwise; $a_{r,lk}^i = 1$ if there is a directed edge from node l to node k in G_r^i and $a_{r,lk}^i = 0$ otherwise. Let $A_p^i = (a_{p,lk}^i)_{|MG_i^c| \times |MG_i^c|}$ and $A_r^i = (a_{r,lk}^i)_{|MG_i^c| \times |MG_i^c|}$ denote the adjacency matrices of G_p^i and G_r^i , respectively. We define the row-normalized transition matrices as $\hat{A}_p^i = D_p^{-1} A_p^i$ and $\hat{A}_r^i = D_r^{-1} A_r^i$, where D_t is a diagonal matrix with

$[D_t]_{ll} = \sum_{k \in MG_i^c} a_{t,lk}^i$ for $t \in \{p, r\}$. The combined transition matrix can be expressed as:

$$P_1^i = \lambda \hat{A}_p^i + (1 - \lambda) \hat{A}_r^i. \quad (2)$$

Prior from Mutual Exclusivity Network. Driver genes often exhibit mutual exclusivity (ME) patterns, meaning that mutations in certain driver gene pairs rarely co-occur within the same sample. This property can help distinguish drivers from passengers. To incorporate this information, we use WeSME [22] to construct an ME network $G_m^c = (V_m^c, E_m^c)$ for each cancer type c based on somatic mutation data. This method employs permutation tests to efficiently compute p -values and false discovery rates (FDR) while preserving sample and gene mutation frequencies. Following the recommended thresholds, we retain significant gene pairs with p -value ≤ 0.01 and FDR ≤ 0.125 for highly-mutated gene pairs (H-H), and p -value ≤ 0.001 and FDR ≤ 0.125 for rarely-mutated to highly-mutated gene pairs (R-H). An edge $(l, k) \in E_m^c$ indicates significant mutual exclusivity between genes l and k . Since statistical methods are stringent and mutation data may be limited, the estimated ME network can be incomplete. Therefore, we use it to provide prior information for random walks on the static networks only when the network scale is sufficiently large (i.e., $|V_m^c| \geq 200$). When this condition is not met, we use a uniform distribution as the prior for the random walk restart term.

For cases where $|V_m^c| \geq 200$, we quantify the mutual exclusivity of each node using two complementary centrality measures: betweenness centrality and harmonic centrality. For each gene $g \in V_m^c$, these centralities are computed as:

$$bc_g = \frac{2}{(|V_m^c| - 1)(|V_m^c| - 2)} \sum_{\substack{k, l \in V_m^c \\ k \neq l \neq g}} \frac{\sigma_{kl}^g}{\sigma_{kl}}, \quad (3)$$

$$hc_g = \frac{1}{|V_m^c| - 1} \sum_{\substack{k \in V_m^c \\ k \neq g}} \frac{1}{d_{kg}}, \quad (4)$$

where σ_{kl}^g is the number of shortest paths between genes k and l passing through gene g , σ_{kl} is the total number of shortest paths between genes k and l , and d_{kg} is the distance between genes k and g in G_m^c . Betweenness centrality captures a node's importance as a bridge in the network, while harmonic centrality (a generalization of closeness centrality to disconnected graphs) measures how central a node is to the overall network structure.

To combine these measures, we first normalize them to a common scale and then compute a weighted combination:

$$\widehat{bc}_g = \frac{bc_g}{\sum_{k \in V_m^c} bc_k}, \quad \widehat{hc}_g = \frac{hc_g}{\sum_{k \in V_m^c} hc_k}, \quad (5)$$

$$c_g = \beta \cdot \widehat{bc}_g + (1 - \beta) \cdot \widehat{hc}_g, \quad (6)$$

where β is a balancing parameter set to 0.8 in this study.

Since the ME network may not include all mutated genes, we impute missing values using the median centrality:

$$\hat{c}_k = \begin{cases} c_k, & k \in V_m^c \cap MG_i^c, \\ \text{median}\{c_g : g \in V_m^c \cap MG_i^c\}, & k \in MG_i^c \setminus V_m^c, \\ 0, & \text{otherwise.} \end{cases} \quad (7)$$

To account for mutation rate bias due to gene length, we introduce a length adjustment factor ℓ_g for each gene g :

$$\ell_g = \exp\left(-\frac{\max(L_g - 10^5, 0)}{10^4}\right), \quad (8)$$

where L_g is the length of gene g in base pairs. This factor down-weights ultra-long genes (longer than 10^5 bp) that have higher background mutation rates. When $|V_m^c| \geq 200$, the initial distribution for random walks on static networks is:

$$s_{0,g}^{(1,i)} = \frac{\hat{c}_g \ell_g}{\sum_{k \in MG_i^c} \hat{c}_k \ell_k}, \quad g \in MG_i^c. \quad (9)$$

When $|V_m^c| < 200$, we use a uniform distribution: $s_{0,g}^{(1,i)} = 1/|MG_i^c|$ for all $g \in MG_i^c$.

Then we utilize $s_0^{(1,i)} \in [0, 1]^{|MG_i^c|}$ as the prior for random walks on G_p^i and G_r^i . To put it another way, the state of each node during random walks can be seen as the probability of being a driver gene. And the initial state is the estimated probabilities from prior information. As the random walks proceed, information from other sources like PPI network and GRN is incorporated to improve the estimation. The iterative process can be expressed as:

$$s_{t+1}^{(1,i)} = \theta(P_1^i)^T s_t^{(1,i)} + (1 - \theta)s_0^{(1,i)}, \quad (10)$$

where $s_t^{(1,i)} \in [0, 1]^{|MG_i^c|}$ denotes the probability distribution of nodes at time t , and θ is the restart probability parameter. Since the random walk with restart can converge to stationary state, the 10 will not update significantly after sufficient iterations. The process converges to a stationary distribution $s^{(1,i)}$ after sufficient iterations. In this study, we set $\theta = 0.85$ and $\lambda = 0.8$.

3.3.2 Random Walks on Dynamic Co-expression Network

Co-expression relationships between genes approximate direct or indirect regulatory interactions, and these patterns may differ between tumor and normal samples. Unlike existing methods that focus solely on differential co-expression, we construct a dynamic co-expression network that integrates information from both tumor and normal samples to capture both tumor-specific and common regulatory patterns. We first compute co-expression correlation matrices R_T^c and R_N^c from the tumor expression matrix X_T^c and normal expression matrix X_N^c , respectively, where $R_{T,jk}^c$ represents the Pearson correlation coefficient between genes j and k across tumor samples. To construct the integrated co-expression network, we define the adjacency matrix $A_{ce}^c \in \{0, 1\}^{|V| \times |V|}$ as:

$$A_{ce,jk}^c = \mathbb{1}\{\max(|R_{T,jk}^c|, |R_{N,jk}^c|) \geq \tau\}, \quad (11)$$

where $\mathbb{1}\{\cdot\}$ is the indicator function, the maximum and absolute value are taken element-wise, and $\tau = 0.5$ is the correlation threshold. This integration preserves strong co-expression relationships (with absolute correlation ≥ 0.5) present in either tumor or normal samples, thereby capturing both condition-specific and shared regulatory patterns.

For sample i , we identify differentially expressed genes (DEGs) by computing the z -score for each gene g :

$$z_g^i = \frac{X_{T,gi}^c - \mu_{N,g}^c}{\sigma_{N,g}^c}, \quad (12)$$

where $X_{T,gi}^c$ is the expression value of gene g in sample i , and $\mu_{N,g}^c$ and $\sigma_{N,g}^c$ are the mean and standard deviation of gene g across normal samples, respectively. We define DEG_i^c as the set of top 500 genes with the highest absolute z -scores.

The induced co-expression subnetwork for sample i is defined as $G_{ce}^i = G_{ce}^c [MG_i^c \cup DEG_i^c]$, which includes both mutated genes and DEGs. The transition matrix for random walks on this network is:

$$P_2^i = D_{ce}^{-1} A_{ce}^i, \quad (13)$$

where A_{ce}^i is the adjacency matrix of G_{ce}^i and D_{ce} is a diagonal matrix with $[D_{ce}]_{ll} = \sum_{k \in MG_i^c \cup DEG_i^c} a_{ce,lk}^i$.

Since driver genes tend to cause larger expression perturbations in downstream genes, we use the absolute z -scores as the prior for the restart distribution:

$$s_{0,g}^{(2,i)} = \frac{|z_g^i|}{\sum_{k \in MG_i^c \cup DEG_i^c} |z_k^i|}, \quad g \in MG_i^c \cup DEG_i^c. \quad (14)$$

The random walk with restart on the co-expression network follows the same iterative scheme as Equation (10):

$$s_{t+1}^{(2,i)} = \theta (P_2^i)^T s_t^{(2,i)} + (1 - \theta) s_0^{(2,i)}, \quad (15)$$

where $s_t^{(2,i)} \in [0, 1]^{|MG_i^c \cup DEG_i^c|}$ is the probability distribution at time t . After convergence, we obtain the stationary state $s^{(2,i)}$.

3.3.3 Integration of Scores from Multiple Networks

The stationary distributions $s^{(1,i)}$ and $s^{(2,i)}$ capture the importance of mutated genes from complementary perspectives: $s^{(1,i)}$ reflects topological importance in static networks and mutual exclusivity patterns, while $s^{(2,i)}$ captures expression perturbation effects. To integrate these scores, we first extract the scores for mutated genes from $s^{(2,i)}$. For notational simplicity, we reuse the symbol $s^{(2,i)} \in [0, 1]^{|MG_i^c|}$ to denote the extracted scores for mutated genes only.

Although both score vectors belong to the $[0, 1]$ range, they may have different distributions. To ensure fair integration, we apply quantile normalization to unify their distributions before combining them:

$$s^{(i)} = \gamma \cdot \text{QN}(s^{(1,i)}) + (1 - \gamma) \cdot \text{QN}(s^{(2,i)}), \quad (16)$$

where $\text{QN}(\cdot)$ denotes the quantile normalization operation and γ is a balancing parameter set to 0.8 in this study. The resulting vector $s^{(i)} \in [0, 1]^{|MG_i^c|}$ provides a coarse estimate of the probability of each mutated gene being a driver gene in sample i .

3.4 Hypergraph Random Walks

The sample-independent random walks described in the previous subsection provide initial driver gene scores by integrating topological and expression perturbation information for each sample individually. However, cancer samples from the same cancer type often share common driver genes and exhibit similar mutational patterns. To leverage these cross-sample similarities, we perform hypergraph-based random walks that incorporate information from multiple related samples. This stage produces both personalized driver gene predictions for individual samples and cohort-level driver gene rankings for each cancer type.

3.4.1 Personalized Driver Gene Identification via Hypergraph Random Walks

For a given sample i of cancer type c , which we refer to as the target sample, we construct a sample-specific hypergraph that integrates information from the target sample and its similar neighbor samples. We define the set of neighbor samples as:

$$NS^i = \{j \in \text{samples of cancer type } c : |MG_j^c \cap MG_i^c| \geq 2, j \neq i\}, \quad (17)$$

where MG_j^c denotes the set of mutated genes in sample j . These neighbor samples share at least two mutated genes with the target sample and may exhibit similar cancer-driving patterns.

We construct a sample-specific hypergraph $\mathcal{H}^i = (\mathcal{V}^i, \mathcal{E}^i)$, where $\mathcal{V}^i = MG_i^c$ is the set of all mutated genes in sample i , and $\mathcal{E}^i = \{e_0, e_1, e_2, \dots, e_N\}$ is the set of hyperedges with each hyperedge corresponding to a sample in $\{i\} \cup NS^i$ (where $|NS^i| = N$) and e_0 representing the target sample i . In this hypergraph, a node $g \in \mathcal{V}^i$ belongs to a hyperedge e_j if and only if gene g is mutated in the corresponding sample. The key advantage of using a hypergraph over a simple graph is that each hyperedge can connect multiple genes simultaneously, naturally capturing the co-mutation patterns across samples. The incidence matrix $H^i \in \{0, 1\}^{|\mathcal{V}^i| \times |\mathcal{E}^i|}$ is defined as:

$$H_{ge}^i = \begin{cases} 1, & g \in e, \\ 0, & \text{otherwise.} \end{cases} \quad (18)$$

To incorporate the driver gene scores obtained from the previous stage, we define a weighted incidence matrix $W^i \in \mathbb{R}^{|\mathcal{V}^i| \times |\mathcal{E}^i|}$ where the weights reflect the importance of genes within each sample:

$$W_{ge}^i = \begin{cases} s_g^j, & g \in e \text{ and } e \text{ corresponds to sample } j, \\ 0, & \text{otherwise.} \end{cases} \quad (19)$$

Here, s_g^j is the driver score of gene g in sample j obtained from Equation (16) in the previous subsection.

For hyperedge weights, we assign higher weights to neighbor samples that are more similar to the target sample, as these samples are expected to provide more relevant information for personalized driver gene prediction. Following Zhang et al. [13], we define the weight of hyperedge e_j (corresponding to sample $j \in NS^i$) as:

$$w_{e_j}^i = \exp\left(-\frac{(1 - \rho_{ij})^2}{2\sigma^2}\right), \quad (20)$$

where ρ_{ij} is the Pearson correlation coefficient between the gene expression profiles of samples i and j , and σ is a bandwidth parameter set to 0.1 in this study. For the target sample's hyperedge e_0 , we set $w_{e_0}^i = 1$. Let W_e^i denote the diagonal matrix with $[W_e^i]_{jj} = w_{e_j}^i$.

Random Walks on Hypergraphs. Random walks on hypergraphs can be naturally defined as a two-step process [23]. Starting from a node u , the walker first selects a hyperedge e from all hyperedges incident to u with probability proportional to the hyperedge weight w_e^i . Then, the walker moves to a node $v \in e$ with probability proportional to the node weight W_{ve}^i in that hyperedge. Formally, the transition probability from node u to node v is:

$$P_{3,uv}^i = \sum_{e \in \mathcal{E}^i} \frac{H_{ue}^i w_e^i}{\sum_{\hat{e} \in \mathcal{E}^i} H_{u\hat{e}}^i w_{\hat{e}}^i} \cdot \frac{W_{ve}^i}{\sum_{\hat{v} \in \mathcal{V}^i} W_{\hat{v}e}^i}. \quad (21)$$

To express this in matrix form, we define:

- D_v^i : diagonal matrix of vertex weighted degrees, where $D_v^i = \text{diag}(d_v^i)$, $d_{v,g}^i = \sum_{e \in \mathcal{E}^i} H_{ge}^i w_e^i$,
- D_{ve}^i : diagonal matrix of hyperedge weighted degrees, where $D_{ve}^i = \text{diag}(d_{ve}^i)$, $d_{ve,e_j}^i = \sum_{g \in \mathcal{V}^i} W_{ge_j}^i$.

Then the transition matrix can be written as:

$$P_3^i = (D_v^i)^{-1} H^i W_e^i (D_{ve}^i)^{-1} (W^i)^T. \quad (22)$$

We perform random walks with restart on the hypergraph \mathcal{H}^i to refine the personalized driver gene scores. The initial distribution is set to uniform over all mutated genes: $p_{0,g}^{(i)} = 1/|\mathcal{V}^i|$ for all $g \in \mathcal{V}^i$. The iterative update follows:

$$p_{t+1}^{(i)} = \alpha (P_3^i)^T p_t^{(i)} + (1 - \alpha) p_0^{(i)}, \quad (23)$$

where $p_t^{(i)} \in [0, 1]^{|\mathcal{V}^i|}$ is the probability distribution at iteration t , and α is the restart probability parameter set to 0.85 in this study. After convergence, we obtain the stationary distribution $p^{(i)}$, which provides the final personalized driver gene scores for sample i . Genes are ranked by their scores $p_g^{(i)}$ in descending order to identify personalized driver gene candidates.

3.4.2 Cohort-level Driver Gene Identification via Hypergraph Random Walks

In addition to personalized predictions, we also identify cohort-level driver genes for each cancer type by aggregating information across all samples. For cancer type c with n_c samples, we construct a cohort-level hypergraph $\mathcal{H}^c = (\mathcal{V}^c, \mathcal{E}^c)$, where:

- \mathcal{V}^c : the set of all genes mutated in at least one sample of cancer type c ,
- $\mathcal{E}^c = \{e_1, e_2, \dots, e_{n_c}\}$: the set of hyperedges, with each hyperedge e_j corresponding to sample j of cancer type c .

The incidence matrix $H^c \in \{0, 1\}^{|\mathcal{V}^c| \times |\mathcal{E}^c|}$ and weighted incidence matrix $W^c \in \mathbb{R}^{|\mathcal{V}^c| \times |\mathcal{E}^c|}$ are defined analogously to the personalized case:

$$H_{ge}^c = \begin{cases} 1, & g \in e, \\ 0, & \text{otherwise,} \end{cases} \quad (24)$$

$$W_{ge}^c = \begin{cases} s_g^j, & g \in e \text{ and } e \text{ corresponds to sample } j, \\ 0, & \text{otherwise.} \end{cases} \quad (25)$$

For cohort-level analysis, we assign equal weight to all hyperedges since we do not prioritize any particular sample. Thus, $w_e^c = 1$ for all $e \in \mathcal{E}^c$. The weighted degree matrices are:

- D_v^c : diagonal matrix with $D_v^c = \text{diag}(d_v^c)$, $d_{v,g}^c = \sum_{e \in \mathcal{E}^c} H_{ge}^c$,
- D_{ve}^c : diagonal matrix with $D_{ve}^c = \text{diag}(d_{ve}^c)$, $d_{ve,e_j}^c = \sum_{g \in \mathcal{V}^c} W_{ge_j}^c$.

The transition matrix is:

$$P_3^c = (D_v^c)^{-1} H^c (D_{ve}^c)^{-1} (W^c)^T. \quad (26)$$

We initialize the random walk with a uniform distribution: $p_{0,g}^{(c)} = 1/|\mathcal{V}^c|$ for all $g \in \mathcal{V}^c$. The iterative process is:

$$p_{t+1}^{(c)} = \alpha(P_3^c)^T p_t^{(c)} + (1 - \alpha)p_0^{(c)}, \quad (27)$$

where $p_t^{(c)} \in [0, 1]^{|\mathcal{V}^c|}$ is the probability distribution at iteration t . After convergence, we obtain the stationary distribution p^c , which provides cohort-level driver gene scores for cancer type c . Genes are ranked by their scores $p_g^{(c)}$ in descending order to identify cohort-level driver genes across all samples of the cancer type.

3.5 Evaluation

Following existing methods in driver gene identification studies, we evaluate the performance of HyperNetWalk and baseline methods by comparing top-ranked predicted driver genes against a reference set of known cancer driver genes from the Cancer Gene Census (CGC) database Tier 1 [24], which contains 584 high-confidence cancer driver genes curated from the literature. For both personalized and cohort-level predictions, we define true driver genes as those present in the intersection of the mutated gene set and CGC Tier 1. To address the issue of partial predictions by certain methods, genes without predicted scores were ranked last to ensure comprehensive coverage of the mutated gene set.

Since driver gene identification methods are primarily used to prioritize candidates for further investigation, we focus on evaluating performance on the top-ranked predictions. Specifically, we assess the top K predicted genes for various values of K , as well as partial area under the curve metrics that emphasize high-confidence predictions.

3.5.1 Evaluation Metrics

We employ the following metrics to quantify prediction performance:

Top-K Metrics. For a given sample or cohort with predicted gene ranking, let TP_K denote the number of true driver genes in the top K predictions, P denote the total number of true driver genes in the evaluation set, and K denote the number of predictions considered. We compute:

- **Precision@K:** the proportion of true driver genes among the top K predictions,

$$\text{Precision@K} = \frac{TP_K}{K}. \quad (28)$$

- **Recall@K:** the proportion of true driver genes recovered in the top K predictions,

$$\text{Recall@K} = \frac{TP_K}{P}. \quad (29)$$

- **F1-score@K:** the harmonic mean of Precision@K and Recall@K,

$$\text{F1@K} = 2 \cdot \frac{\text{Precision@K} \cdot \text{Recall@K}}{\text{Precision@K} + \text{Recall@K}}. \quad (30)$$

Area Under Curve Metrics. To provide a comprehensive assessment across all possible thresholds, we compute:

- **Area Under the Precision-Recall Curve (AUPRC):** summarizes the trade-off between precision and recall across all ranking thresholds. This metric is particularly informative for imbalanced datasets where driver genes are much rarer than passenger genes.
- **Area Under the Receiver Operating Characteristic Curve (AUROC):** measures the ability to distinguish between driver and non-driver genes across all thresholds.
- **Partial AUPRC (pAUPRC):** the area under the precision-recall curve for the top K predictions, defined as the AUPRC computed only for predictions up to rank K . This metric emphasizes performance on high-confidence predictions where recall is at most $R_{max} = K/M$, where M is the total number of mutated genes.
- **Partial AUROC (pAUROC):** the area under the ROC curve for the top K predictions, computed analogously to pAUPRC. This metric focuses on the false positive rate within the top-ranked predictions.

For partial metrics, we set K to be the top 10% of mutated genes, which emphasizes the model’s ability to prioritize the most likely driver genes—the primary use case in practice.

3.5.2 Personalized Evaluation Strategy

For personalized driver gene identification, we employ a ranking-evaluation-aggregation (REA) strategy [12]. Following this approach, we only evaluate samples that have at least three true driver genes in their mutated gene sets (i.e., $|MG_i^c \cap \text{CGC Tier 1}| \geq 3$). Since samples from different cancer types may have different distributions of true driver gene counts, for each cancer type c , we evaluate the top N_c predictions for each sample, where:

$$N_c = 2 \cdot \text{median}\{|MG_i^c \cap \text{CGC Tier 1}| : i \in \text{evaluated samples of type } c\}. \quad (31)$$

For samples with fewer than N_c mutated genes (i.e., $|MG_i^c| < N_c$), Precision@K and Recall@K metrics for $K > |MG_i^c|$ exclude these samples from calculation. We aggregate the evaluation metrics (Precision@K, Recall@K, and F1@K for various K values) across all evaluated samples by computing their mean to obtain the overall performance for personalized driver gene identification.

3.5.3 Cohort-level Evaluation Strategy

For cohort-level driver gene identification, we evaluate the ranking of all mutated genes in each cancer type c against the reference set $\mathcal{V}^c \cap \text{CGC Tier 1}$. We compute Precision@K, Recall@K, F1@K for various values of K (e.g., $K \in \{10, 20, 30, 50, 100\}$), as well as AUPRC, AUROC, pAUPRC, and pAUROC. For partial metrics at the cohort level, we set K to be the top 10% of all mutated genes in cancer type c , which typically corresponds to several hundred genes depending on the cancer type.

4. Discussion

Identifying cancer driver genes is a fundamental step toward precision oncology. In this study, we presented HyperNetWalk, a unified framework that integrates multi-omics data with static and dynamic

biological networks to identify driver genes at both the personalized and cohort levels. By leveraging hypergraph diffusion, our method effectively captures high-order correlations across patients while preserving individual-specific mutational contexts.

Our extensive evaluation on 12 TCGA cancer types demonstrates that HyperNetWalk achieves performance comparable to, and often surpassing, state-of-the-art methods. A key strength of our approach is its versatility. While cohort-based methods like DriverMP excel at capturing population-level signals, they often miss rare, patient-specific drivers. Conversely, personalized methods like DawnRank are sensitive to individual mutations but may lack the statistical power to filter out noise without cohort-level guidance. HyperNetWalk bridges this gap, delivering high-confidence predictions in both scenarios.

The cross-cancer specificity analysis further validates the biological relevance of our predictions. The strong diagonal pattern in the specificity matrix confirms that HyperNetWalk does not merely prioritize general, high-frequency drivers (like *TP53*) but successfully uncovers tissue-specific driver landscapes. This is particularly valuable for unraveling the heterogeneity of cancer, where different patients with the same tumor type may be driven by distinct molecular mechanisms.

Despite these promising results, several limitations remain. First, the PPI network used in this study, while extensive, is inherently incomplete and prone to false positives. Furthermore, standard PPI networks are static and do not capture the dynamic rewiring of interactions that occurs during tumorigenesis. Future iterations of HyperNetWalk could incorporate context-specific or dynamic PPI networks to better model the tumor microenvironment.

Second, our current model simplifies gene regulation by treating it as a pairwise interaction graph. While we incorporate a dynamic co-expression network to capture perturbation effects, we do not fully model the complex, non-linear combinatorial interactions among multiple proteins. Utilizing hypergraph-based representations for protein complexes or pathway-level interactions could provide a more faithful model of cellular logic.

Third, while we utilize the magnitude of differential expression (z -scores) to weight the random walk, we do not currently exploit the direction of regulation (up- or down-regulation). Distinguishing between oncogenes (often up-regulated) and tumor suppressors (often down-regulated or deleted) could further refine our scoring system. Integrating copy number variation (CNV) data more explicitly could also help address this limitation.

Finally, although HyperNetWalk is computationally efficient for the datasets analyzed, scaling hypergraph diffusion to extremely large pan-cancer cohorts with tens of thousands of samples remains a challenge. Future work will focus on optimizing the hypergraph construction and diffusion algorithms to enable real-time analysis of massive clinical datasets.

Data Availability

The results presented in this study are in part based upon data generated by the TCGA Research Network (<https://www.cancer.gov/tcga>). TCGA multi-omic data, including somatic mutations, gene expression, methylation, and copy number variation, were accessed through the Genomic Data Commons (GDC) Data Portal. All data used in this study are publicly available. Processed data and analysis scripts necessary to reproduce the main results of this work are available at: <https://github.com/xqxu921/HyperNetWalk>. Additional intermediate data products are available from the corresponding author upon reasonable request.

Acknowledgements

This work has been supported by the National Key Research and Development Program of China (No. 2020YFA0712400); National Natural Science Foundation of China (No. 12231018, 62202269). The results published here are in whole or part based upon data generated by The Cancer Genome Atlas (TCGA) Research Network (<https://www.cancer.gov/tcga>). We are grateful to the TCGA Research Network and to all patients and their families for their invaluable contributions to cancer research.

References

- [1] Michael S. Lawrence, Petar Stojanov, Paz Polak, Gregory V. Kryukov, Kristian Cibulskis, Andrey Sivachenko, Scott L. Carter, Chip Stewart, Craig H. Mermel, Steven A. Roberts, et al. Mutational heterogeneity in cancer and the search for new cancer-associated genes. *Nature*, 499(7457):214–218, 2013.
- [2] Yi Han, Juze Yang, Xinyi Qian, Wei-Chung Cheng, Shu-Hsuan Liu, Xing Hua, Liyuan Zhou, Yaning Yang, Qingbiao Wu, Pengyuan Liu, et al. Driverml: a machine learning algorithm for identifying driver genes in cancer sequencing studies. *Nucleic Acids Research*, 47(8):e45–e45, 2019.
- [3] Loris Mularoni, Radhakrishnan Sabarinathan, Jordi Deu-Pons, Abel Gonzalez-Perez, and Núria López-Bigas. Oncodrivefml: a general framework to identify coding and non-coding regions with cancer driver mutations. *Genome biology*, 17(1):128, 2016.
- [4] Felix Dietlein, Donat Wenghorn, Amaro Taylor-Weiner, André Richters, Brendan Reardon, David Liu, Eric S Lander, Eliezer M Van Allen, and Shamil R Sunyaev. Identification of cancer driver genes based on nucleotide context. *Nature genetics*, 52(2):208–218, 2020.
- [5] Roman Schulte-Sasse, Stefan Budach, Denes Hnisz, and Annalisa Marsico. Integration of multi-omics data with graph convolutional networks to identify new cancer genes and their associated molecular mechanisms. *Nature Machine Intelligence*, 3(6):513–526, 2021.
- [6] Peiting Shi, Junmin Han, Yinghao Zhang, Guanpu Li, and Xionghui Zhou. Imi-driver: integrating multi-level gene networks and multi-omics for cancer driver gene identification. *PLOS Computational Biology*, 20(8):e1012389, 2024.
- [7] Mark DM Leiserson, Fabio Vandin, Hsin-Ta Wu, Jason R Dobson, Jonathan V Eldridge, Jacob L Thomas, Alexandra Papoutsaki, Younhun Kim, Beifang Niu, Michael McLellan, et al. Pan-cancer network analysis identifies combinations of rare somatic mutations across pathways and protein complexes. *Nature genetics*, 47(2):106–114, 2015.
- [8] Ali Bashashati, Gholamreza Haffari, Jiarui Ding, Gavin Ha, Kenneth Lui, Jamie Rosner, David G Huntsman, Carlos Caldas, Samuel A Aparicio, and Sohrab P Shah. Drivernet: uncovering the impact of somatic driver mutations on transcriptional networks in cancer. *Genome biology*, 13(12):R124, 2012.
- [9] Bert Vogelstein, Nickolas Papadopoulos, Victor E. Velculescu, Shibin Zhou, Luis A. Diaz, and Kenneth W. Kinzler. Cancer genome landscapes. *Science*, 339(6127):1546–1558, 2013.
- [10] Jack P Hou and Jian Ma. Dawnrank: discovering personalized driver genes in cancer. *Genome medicine*, 6(7):56, 2014.

- [11] Wei-Feng Guo, Shao-Wu Zhang, Li-Li Liu, Fei Liu, Qian-Qian Shi, Lei Zhang, Ying Tang, Tao Zeng, and Luonan Chen. Discovering personalized driver mutation profiles of single samples in cancer by network control strategy. *Bioinformatics*, 34(11):1893–1903, 2018.
- [12] Cesim Erten, Aissa Houdjedj, Hilal Kazan, and Ahmed Amine Taleb Bahmed. Personadrive: a method for the identification and prioritization of personalized cancer drivers. *Bioinformatics*, 38(13):3407–3414, 2022.
- [13] Naiqian Zhang, Fubin Ma, Dong Guo, Yuxuan Pang, Chenye Wang, Yusen Zhang, Xiaoqi Zheng, and Mingyi Wang. A novel hypergraph model for identifying and prioritizing personalized drivers in cancer. *PLOS Computational Biology*, 20(4):e1012068, 2024.
- [14] Yangyang Liu, Jiyun Han, Tongxin Kong, Nannan Xiao, Qinglin Mei, and Juntao Liu. Drivermp enables improved identification of cancer driver genes. *GigaScience*, 12:giad106, 2023.
- [15] Yuhe Wang, Suoqin Jin, and Xiufen Zou. Pitch: A pathway-induced prioritization of personalized cancer driver genes based on higher-order interactions. *IEEE Journal of Biomedical and Health Informatics*, 2025.
- [16] Gal Dinstag and Ron Shamir. Prodigy: personalized prioritization of driver genes. *Bioinformatics*, 36(6):1831–1839, 2020.
- [17] Chenye Wang, Junhan Shi, Jiansheng Cai, Yusen Zhang, Xiaoqi Zheng, and Naiqian Zhang. Driver-rwh: discovering cancer driver genes by random walk on a gene mutation hypergraph. *BMC bioinformatics*, 23(1):277, 2022.
- [18] Junrong Song, Wei Peng, and Feng Wang. A random walk-based method to identify driver genes by integrating the subcellular localization and variation frequency into bipartite graph. *BMC bioinformatics*, 20(1):238, 2019.
- [19] Mary J Goldman, Brian Craft, Mim Hastie, Kristupas Repečka, Fran McDade, Akhil Kamath, Ayan Banerjee, Yunhai Luo, Dave Rogers, Angela N Brooks, et al. Visualizing and interpreting cancer genomics data via the xena platform. *Nature biotechnology*, 38(6):675–678, 2020.
- [20] Damian Szklarczyk, Rebecca Kirsch, Mikaela Koutrouli, Katerina Nastou, Farrokh Mehryary, Radja Hachilif, Annika L Gable, Tao Fang, Nadezhda T Doncheva, Sampo Pyysalo, et al. The string database in 2023: protein–protein association networks and functional enrichment analyses for any sequenced genome of interest. *Nucleic acids research*, 51(D1):D638–D646, 2023.
- [21] Bowen Li, Chuanyuan Wang, Yijuan Wang, Pengpai Li, and Zhi-Ping Liu. Regnetwork 2025: an integrative data repository for gene regulatory networks in human and mouse. *Nucleic Acids Research*, page gkaf779, 2025.
- [22] Yoo-Ah Kim, Sanna Madan, and Teresa M Przytycka. Wesme: uncovering mutual exclusivity of cancer drivers and beyond. *Bioinformatics*, 33(6):814–821, 2017.
- [23] Timoteo Carletti, Federico Battiston, Giulia Cencetti, and Duccio Fanelli. Random walks on hypergraphs. *Physical review E*, 101(2):022308, 2020.
- [24] Zbyslaw Sondka, Sally Bamford, Charlotte G Cole, Sari A Ward, Ian Dunham, and Simon A Forbes. The cosmic cancer gene census: describing genetic dysfunction across all human cancers. *Nature Reviews Cancer*, 18(11):696–705, 2018.

Supplementary Materials

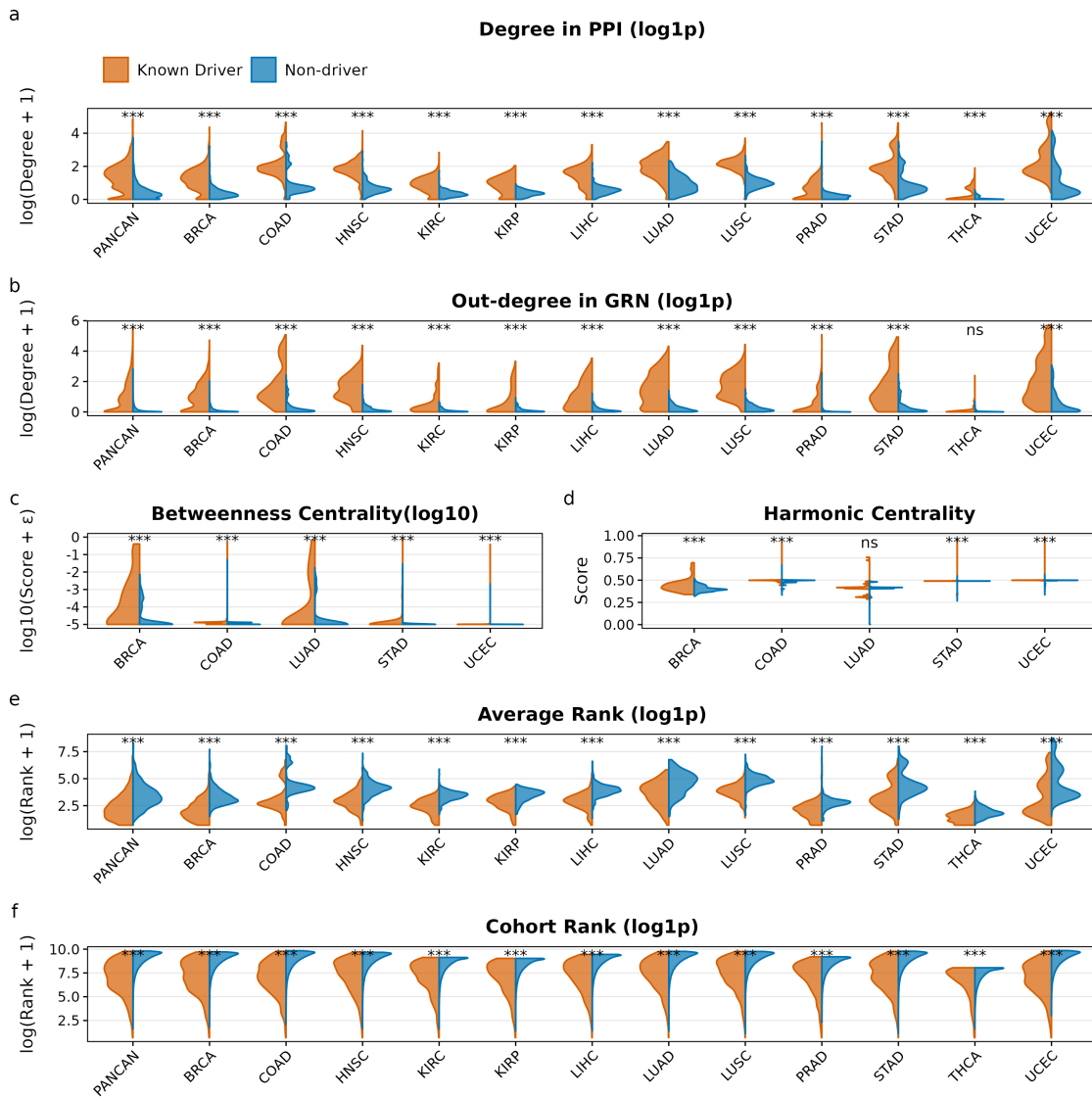


Figure S1. Known driver genes exhibit distinct network topology and ranking characteristics across cancer types. Comparison of network properties and HyperNetWalk ranking metrics between known driver genes (from CGC Tier 1) and non-driver genes across 12 TCGA cancer types and pan-cancer cohort. **(a)** Degree in PPI network: Known drivers show significantly higher connectivity than non-drivers, consistent with their role as network hubs. **(b)** Out-degree in GRN: Known drivers generally exhibit higher regulatory capacity, indicating greater influence on downstream targets. The difference in THCA is not statistically significant (ns). **(c)** Betweenness centrality in ME network: Known drivers show significantly higher betweenness centrality across five cancer types with sufficiently large ME networks ($|V_m^c| \geq 200$). **(d)** Harmonic centrality in ME network: Known drivers exhibit higher harmonic centrality compared to non-drivers in most cancer types, with LUAD as the exception. **(e)** Average personalized rank: Known drivers consistently achieve significantly lower (better) average ranks across individual patient samples. **(f)** Cohort-level rank: Known drivers are ranked significantly higher (lower rank values) at the cohort level across all cancer types. Y-axes are log-transformed (log_{1p}: $\log(\text{value} + 1)$ or log₁₀: $\log_{10}(\text{value} + \epsilon)$, where $\epsilon = 10^{-5}$) for visualization clarity. Statistical significance assessed on original values using Wilcoxon rank-sum test: *** $p < 0.001$; ** $p < 0.01$; * $p < 0.05$; ns, not significant.

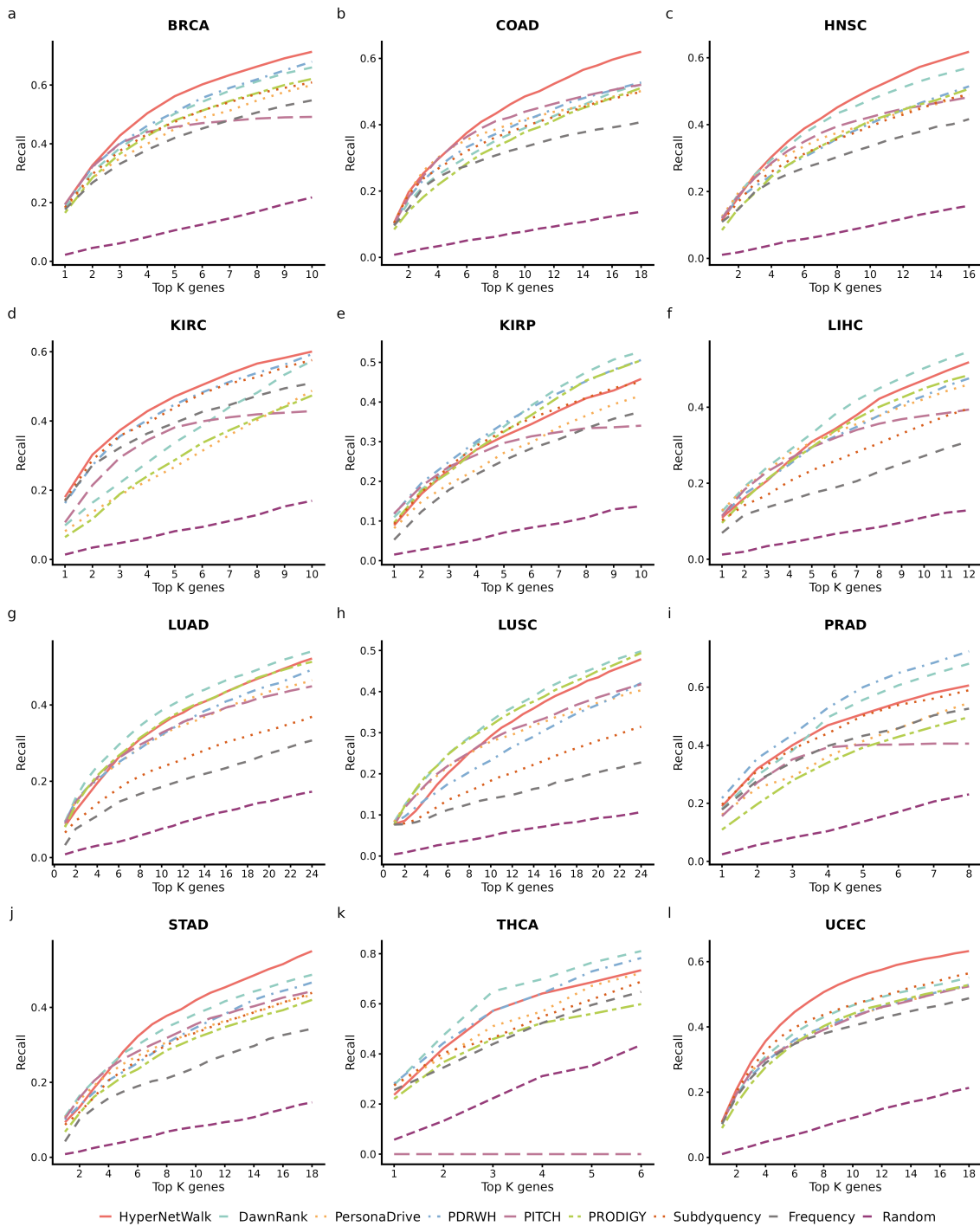


Figure S2. Personalized prediction performance: Recall@K across cancer types. Recall@K curves for HyperNetWalk and baseline methods on personalized driver gene identification across 12 TCGA cancer types. Panels (a–l) represent different cancer types, showing how the proportion of recovered true drivers increases with K. Performance is evaluated using cancer type-specific cutoffs N_c (see Methods). HyperNetWalk demonstrates strong recall performance, effectively capturing the majority of known drivers within top-ranked predictions across diverse cancer types.

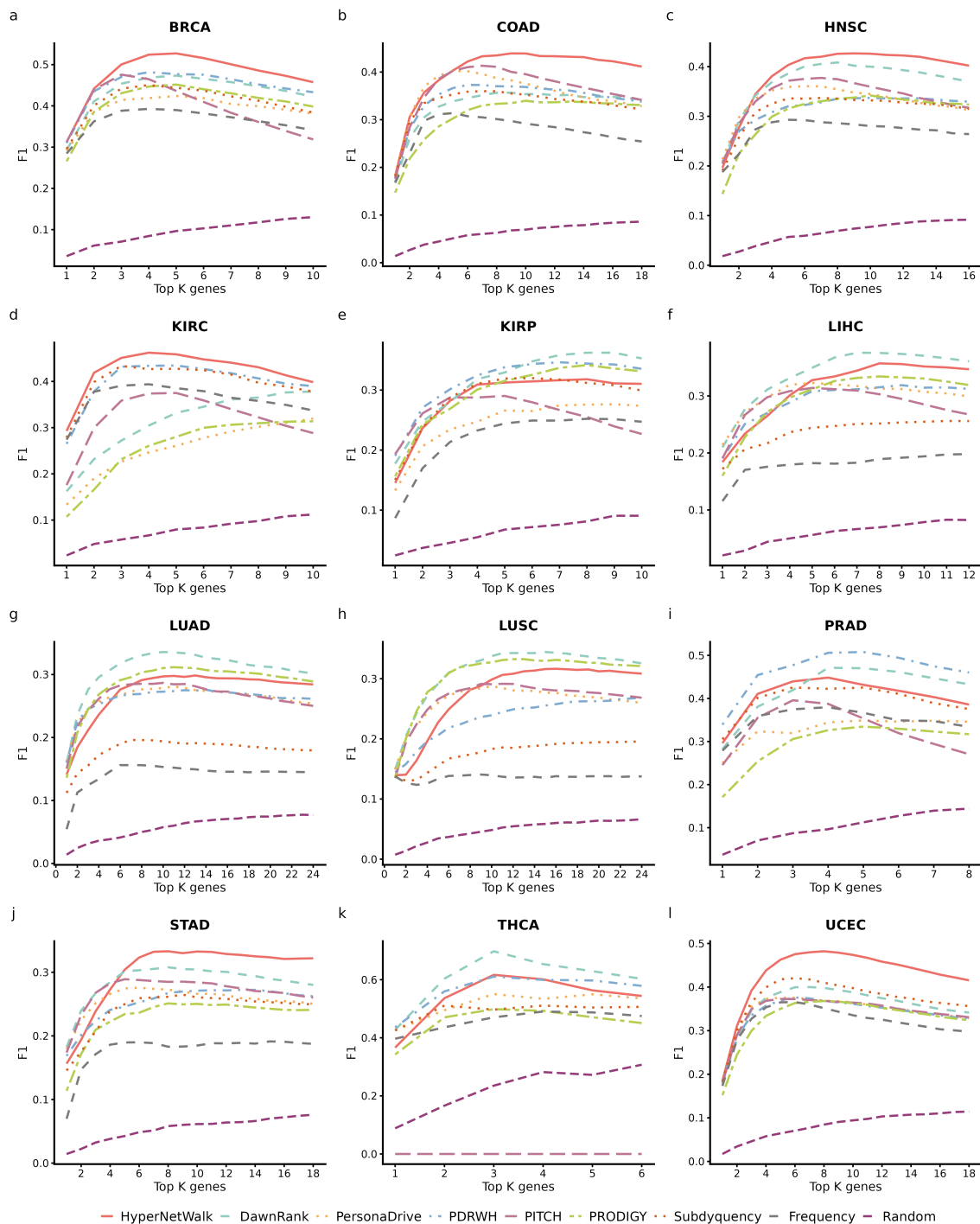


Figure S3. Personalized prediction performance: F1-score@K across cancer types. F1-score@K curves for HyperNetWalk and baseline methods on personalized driver gene identification across 12 TCGA cancer types. Panels (a–l) represent different cancer types, displaying the harmonic mean of precision and recall. Performance is evaluated using cancer type-specific cutoffs N_c (see Methods). HyperNetWalk achieves the highest or near-highest F1 scores in the majority of cancer types, indicating balanced performance in both precision and recall for patient-specific predictions.

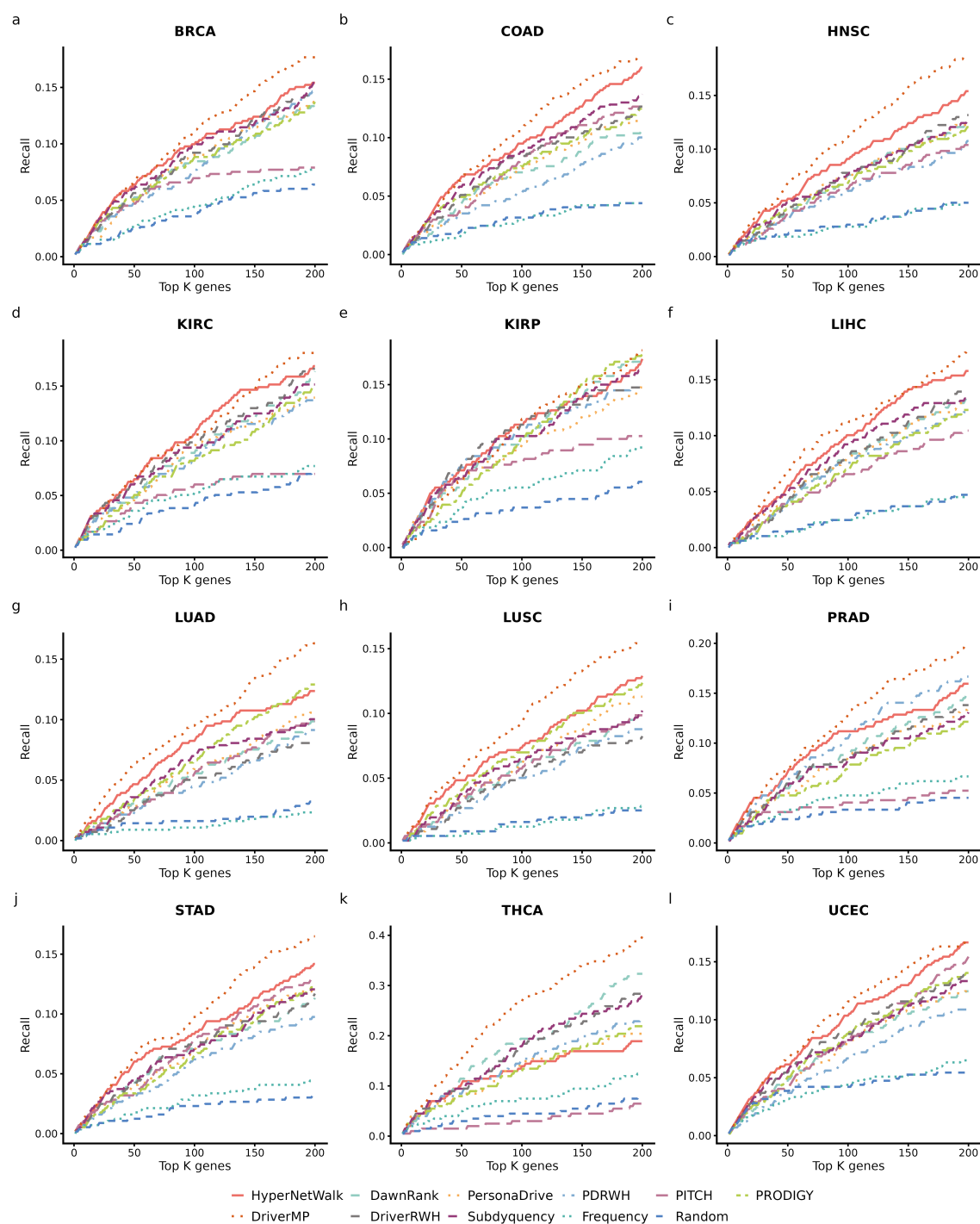


Figure S4. Cohort-level prediction performance: Recall@K across cancer types. Recall@K curves for HyperNetWalk and baseline methods on cohort-level driver gene identification across 12 TCGA cancer types. Panels (a–l) represent different cancer types, showing the recovery rate of known cohort-level drivers. Performance is evaluated on the top 200 ranked genes. HyperNetWalk demonstrates strong recall, effectively identifying the majority of population-level drivers within top-ranked predictions.

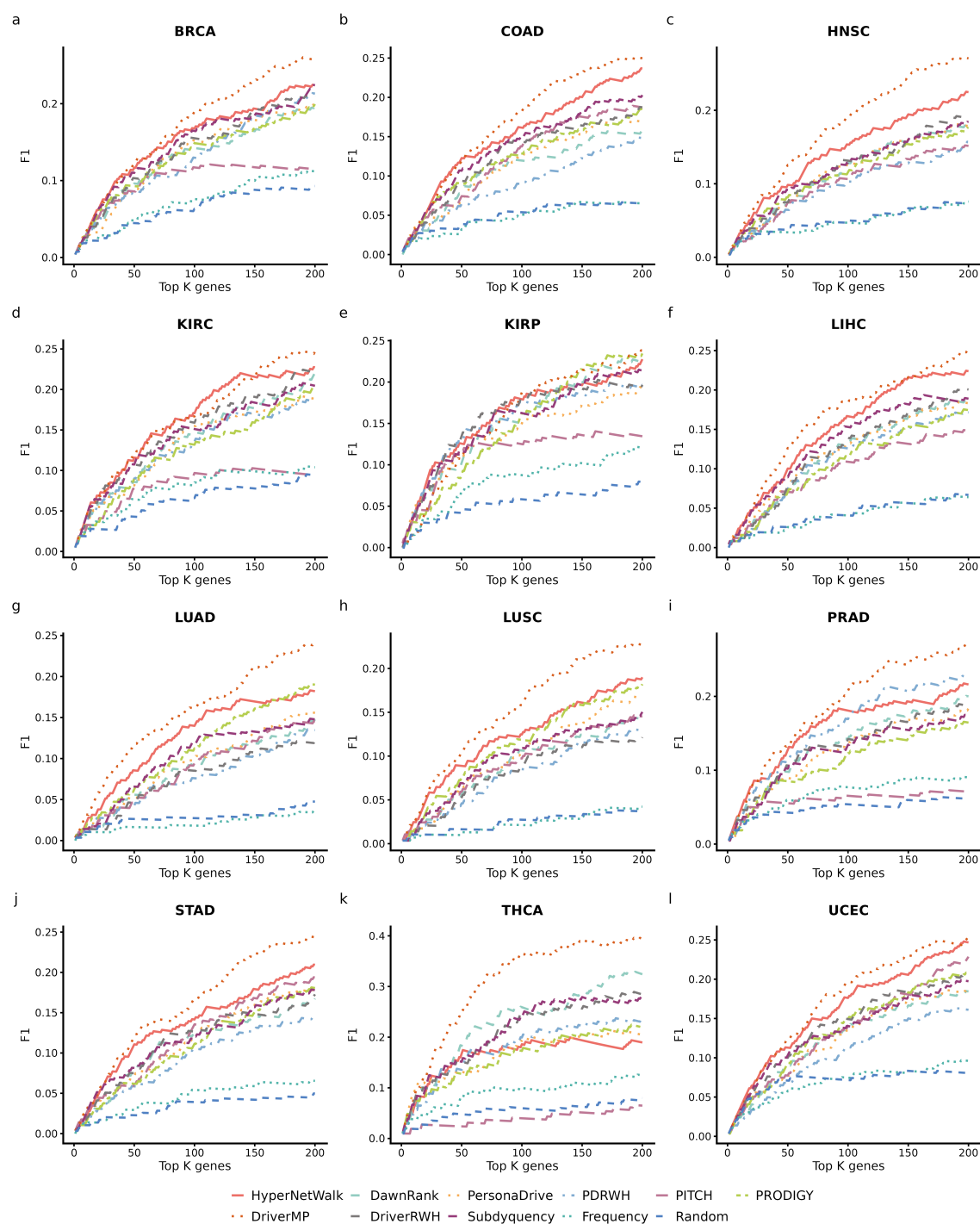


Figure S5. Cohort-level prediction performance: F1-score@K across cancer types. F1-score@K curves for HyperNetWalk and baseline methods on cohort-level driver gene identification across 12 TCGA cancer types. Panels (a-l) represent different cancer types, showing the balanced performance metric combining precision and recall. Performance is evaluated on the top 200 ranked genes. HyperNetWalk maintains consistently high F1 scores, ranking among the top two methods across all cancer types.

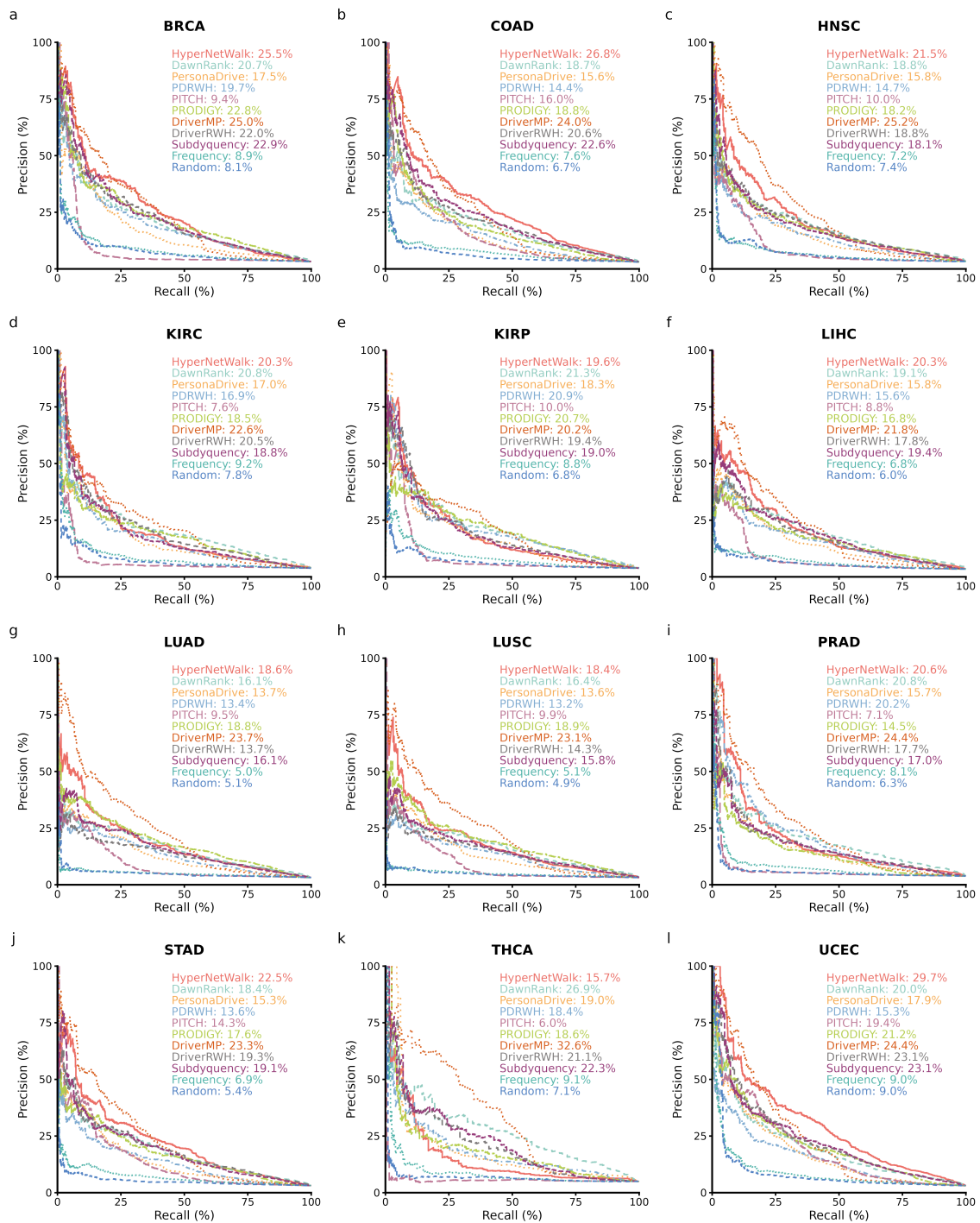


Figure S6. Cohort-level prediction performance: Precision-recall curves across cancer types. Precision-recall (PR) curves for HyperNetWalk and baseline methods on cohort-level predictions across 12 TCGA cancer types. Panels (a–l) represent different cancer types. The curves illustrate the trade-off between precision and recall across the entire ranking list, with the Area Under the Curve (AUPRC) quantifying the global retrieval performance.

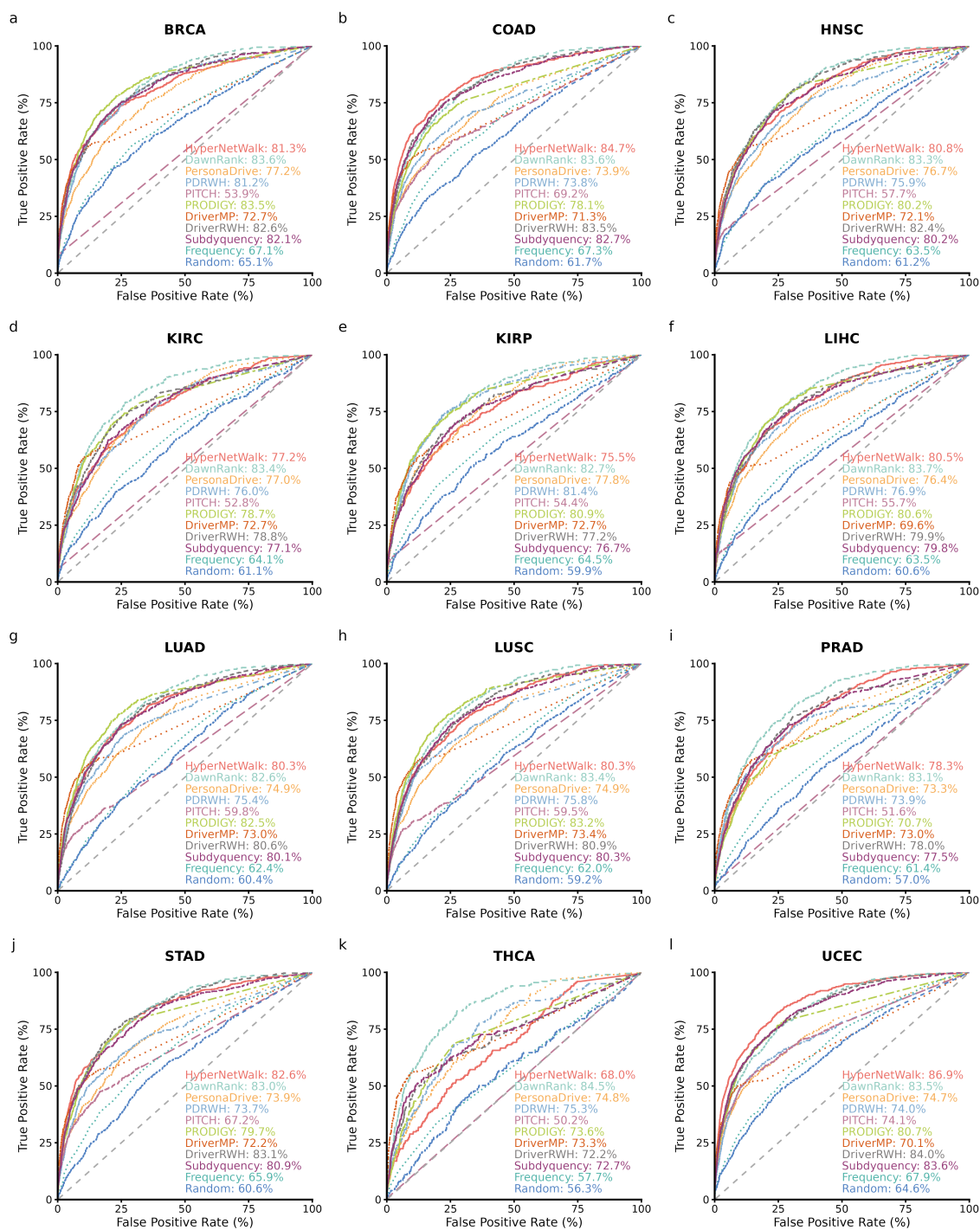


Figure S7. Cohort-level prediction performance: ROC curves across cancer types. Receiver Operating Characteristic (ROC) curves for HyperNetWalk and baseline methods on cohort-level predictions across 12 TCGA cancer types. Panels (a-l) represent different cancer types. The plots display the True Positive Rate versus the False Positive Rate across all possible thresholds. The Area Under the ROC Curve (AUROC) serves as a metric for the overall classification capability of each method.

Table S1. Summary of TCGA datasets analyzed in this study. For each cancer type, the table reports the number of mutation samples, mutated genes, tumor expression samples, normal expression samples, and expressed genes.

Cancer Type	Mut. Samples	Mut. Genes	Expr. Tumor	Expr. Normal	Expr. Genes
BRCA	985	16,662	1,081	99	59,427
COAD	440	18,654	455	41	59,427
HNSC	510	16,509	515	44	59,427
KIRC	379	10,929	529	72	59,427
KIRP	279	9,920	289	32	59,427
LIHC	371	14,340	369	50	59,427
LUAD	575	17,705	513	58	59,427
LUSC	491	17,623	496	51	59,427
PRAD	495	11,075	483	51	59,427
STAD	431	18,003	410	36	59,427
THCA	496	4,163	500	57	59,427
UCEC	515	18,993	539	35	59,427

Table S2. Detailed performance metrics across 12 cancer types. The **top two** performing methods in each category are highlighted in **bold**.

Cancer	Method	AUPRC	AUROC	pAUPRC	pAUROC
BRCA	HyperNetWalk	25.4803	81.2693	7.5471	4.1150
	DawnRank	20.6674	83.6036	5.7897	3.5678
	PersonaDrive	17.4972	77.1913	5.8011	2.9653
	PDRWH	19.7412	81.2402	5.5339	3.4345
	PITCH	9.3756	53.8775	5.3061	1.2224
	PRODIGY	22.7907	83.5348	6.3305	3.8369
	DriverMP	25.0232	72.6634	7.6942	4.0023
	DriverRWH	22.0250	82.6275	6.0623	3.7451
	Subdyquency	22.9446	82.1258	6.9674	3.7564
	Frequency	8.9295	67.0761	2.9495	1.8151
Random	8.1009	65.0887	2.5625	1.7175	
COAD	HyperNetWalk	26.8138	84.6961	7.3805	4.4117
	DawnRank	18.6598	83.5618	4.6025	3.6264
	PersonaDrive	15.5902	73.8818	5.3001	2.9088
	PDRWH	14.3864	73.7959	3.9681	3.0402
	PITCH	15.9890	69.1768	5.7691	2.8821
	PRODIGY	18.7655	78.0668	5.9159	3.3641
	DriverMP	23.9708	71.2505	7.6021	3.8405
	DriverRWH	20.5991	83.5205	5.6610	3.7957
	Subdyquency	22.6005	82.7248	6.6609	3.8859
	Frequency	7.5797	67.3362	1.9986	1.7015

Continued on next page

Table S2 continued from previous page

Cancer	Method	AUPRC	AUROC	pAUPRC	pAUROC
	Random	6.6744	61.6555	2.2591	1.4415
HNSC	HyperNetWalk	21.5240	80.8194	6.6465	3.4808
	DawnRank	18.7737	83.2789	4.6574	3.4537
	PersonaDrive	15.8218	76.7495	5.0301	2.8604
	PDRWH	14.7099	75.8574	4.0560	2.8846
	PITCH	9.9548	57.7164	4.1528	1.8440
	PRODIGY	18.2345	80.1518	5.1613	3.2629
	DriverMP	25.2046	72.1133	7.8485	3.8689
	DriverRWH	18.8231	82.3577	4.8204	3.4051
	Subdyquency	18.1348	80.2005	5.4105	3.1900
	Frequency	7.2362	63.5236	2.1702	1.5163
	Random	7.3531	61.2460	2.3613	1.5648
KIRC	HyperNetWalk	20.2891	77.1776	6.7186	3.0118
	DawnRank	20.8125	83.3948	5.1721	3.3058
	PersonaDrive	17.0002	76.9696	5.3437	2.6384
	PDRWH	16.8555	76.0445	5.1409	2.8105
	PITCH	7.6363	52.7950	3.4109	1.0191
	PRODIGY	18.5214	78.7248	4.4855	3.1861
	DriverMP	22.6236	72.6773	6.7681	3.6615
	DriverRWH	20.4725	78.7539	6.1191	3.1474
	Subdyquency	18.7876	77.1049	6.1406	2.8293
	Frequency	9.1799	64.1355	3.1690	1.5548
	Random	7.8294	61.0796	2.5074	1.3861
KIRP	HyperNetWalk	19.6238	75.4812	6.6002	2.9160
	DawnRank	21.2999	82.6854	5.2758	3.4111
	PersonaDrive	18.2545	77.7912	5.6218	2.8919
	PDRWH	20.8899	81.3844	6.1145	3.1920
	PITCH	9.9748	54.4368	4.9920	1.3177
	PRODIGY	20.6657	80.9101	4.3199	3.5143
	DriverMP	20.1838	72.7432	4.2842	3.6418
	DriverRWH	19.4042	77.2131	5.9889	3.0037
	Subdyquency	19.0199	76.6626	6.0668	2.9216
	Frequency	8.8136	64.5435	2.3315	1.6623
	Random	6.8096	59.9390	1.6098	1.2976
LIHC	HyperNetWalk	20.2908	80.4896	5.6620	3.3440
	DawnRank	19.0935	83.6544	4.0336	3.5334
	PersonaDrive	15.8156	76.4113	4.6455	2.8222
	PDRWH	15.6188	76.9077	3.9421	2.9988
	PITCH	8.8188	55.6659	3.5606	1.5142
	PRODIGY	16.8332	80.6378	3.7414	3.1395

Continued on next page

Table S2 continued from previous page

Cancer	Method	AUPRC	AUROC	pAUPRC	pAUROC
	DriverMP	21.7538	69.5732	6.5333	3.6383
	DriverRWH	17.7994	79.8746	4.1476	3.2803
	Subdyquency	19.4046	79.8007	5.1794	3.4620
	Frequency	6.7574	63.4520	1.4197	1.4786
	Random	6.0100	60.6168	1.3856	1.2929
LUAD	HyperNetWalk	18.6417	80.2941	5.3429	3.3496
	DawnRank	16.1400	82.6039	3.1430	3.3568
	PersonaDrive	13.6696	74.8776	3.5608	2.7756
	PDRWH	13.4357	75.4279	3.0191	2.9232
	PITCH	9.4907	59.7628	3.3676	2.0677
	PRODIGY	18.8404	82.4545	4.2192	3.5589
	DriverMP	23.7102	72.9726	7.3186	3.9586
	DriverRWH	13.7222	80.5867	2.8601	2.9190
	Subdyquency	16.1424	80.0912	3.7968	3.2167
	Frequency	5.0053	62.3764	0.8506	1.0213
	Random	5.0893	60.4425	1.1495	1.0097
LUSC	HyperNetWalk	18.4472	80.2994	5.4012	3.3264
	DawnRank	16.4412	83.3506	3.3752	3.3847
	PersonaDrive	13.5749	74.8753	3.7004	2.6700
	PDRWH	13.1651	75.8158	2.9457	2.8824
	PITCH	9.9442	59.5337	3.8279	2.1703
	PRODIGY	18.8684	83.1786	4.4225	3.5603
	DriverMP	23.1060	73.3715	6.6103	4.0148
	DriverRWH	14.3422	80.8843	2.9322	3.0406
	Subdyquency	15.8390	80.2518	3.7942	3.1727
	Frequency	5.1292	61.9514	0.9891	1.0716
	Random	4.9189	59.2164	1.0533	1.0471
PRAD	HyperNetWalk	20.5699	78.3370	7.4232	2.8668
	DawnRank	20.7776	83.1029	5.5373	3.2648
	PersonaDrive	15.6630	73.3307	4.7334	2.6485
	PDRWH	20.1778	73.8626	5.9284	3.2376
	PITCH	7.1094	51.5721	2.7804	0.7965
	PRODIGY	14.4503	70.7383	4.2900	2.5108
	DriverMP	24.3551	73.0043	7.6163	3.5586
	DriverRWH	17.7447	78.0075	5.4332	2.7940
	Subdyquency	17.0478	77.4861	4.8777	2.7845
	Frequency	8.1444	61.3793	2.7145	1.3344
	Random	6.3115	56.9672	1.9504	0.9096
STAD	HyperNetWalk	22.5414	82.5654	6.1486	3.9693
	DawnRank	18.3888	83.0496	4.3497	3.5074

Continued on next page

Table S2 continued from previous page

Cancer	Method	AUPRC	AUROC	pAUPRC	pAUROC
	PersonaDrive	15.2824	73.8817	5.0363	2.7979
	PDRWH	13.6437	73.7311	3.6098	2.9040
	PITCH	14.2883	67.2239	5.0873	2.7145
	PRODIGY	17.5802	79.7116	4.1227	3.3876
	DriverMP	23.3494	72.2232	7.2219	3.8362
	DriverRWH	19.2532	83.0937	4.8809	3.5833
	Subdyquency	19.0566	80.8929	5.2977	3.5283
	Frequency	6.9041	65.9275	1.5518	1.5838
	Random	5.4022	60.5502	1.3256	1.1385
THCA	HyperNetWalk	15.6691	68.0468	5.9488	1.9975
	DawnRank	26.9458	84.5044	5.7363	3.6656
	PersonaDrive	19.0038	74.8262	7.2114	2.2464
	PDRWH	18.3907	75.2947	5.3211	2.4048
	PITCH	5.9932	50.2230	1.2139	0.5423
	PRODIGY	18.6036	73.6402	5.7196	2.4470
	DriverMP	32.6356	73.3444	7.9033	4.2768
	DriverRWH	21.1071	72.2442	6.0728	2.9504
	Subdyquency	22.2863	72.7361	6.3717	3.1891
	Frequency	9.1096	57.7391	3.0265	1.2409
	Random	7.0905	56.3075	1.6348	0.7565
UCEC	HyperNetWalk	29.6711	86.8711	8.1957	4.6300
	DawnRank	20.0327	83.5309	5.6616	3.6522
	PersonaDrive	17.8536	74.7402	5.9574	3.2234
	PDRWH	15.3431	73.9939	4.4606	3.1877
	PITCH	19.4374	74.1155	5.8381	3.4561
	PRODIGY	21.2190	80.6778	5.9566	3.8138
	DriverMP	24.4242	70.1434	8.3346	3.8432
	DriverRWH	23.0857	83.9541	6.9198	3.9201
	Subdyquency	23.1245	83.5616	6.9551	4.0045
	Frequency	9.0019	67.9353	3.3687	1.7962
	Random	8.9515	64.6365	4.0235	1.5787